TREND

Trapped Radiation Environment Model Development

Technical Note 3

Implementation of CRRESPRO in UNIRAD

ESTEC Contract No. 9828/92/NL/FM[1]

D. Heynderickx (BIRA)

March 1995

[1]ESA Technical Management: E.J. Daly (WMA)

Contents

List of Figures

List of Tables

Introduction

The NASA models AP-8 and AE-8 still are the most widely used empirical descriptions of the trapped particle population in the Earth's radiation belts. Since these models were built more than twenty years ago and need updating, new missions have been designed and flown recently to provide new data.

The most extensive of these missions to date is CRRES. This satellite carried a large complement of instruments designed to study different aspects of the radiation belt environment. For the TREND study, the particle detectors onboard CRRES are of particular importance. The data obtained with the MEA electron detector have been studied by Rodgers (1994) and have resulted in a new trapped electron model, which has been integrated in the `UNIRAD` software by BIRA/IASB.

In this technical note, we describe the new proton flux model CRRESPRO developed by Phillips Lab from the PROTEL instrument onboard CRRES. Originally it was expected that BIRA/IASB would obtain the PROTEL data and produce its own low altitude proton model. Instead, BIRA/IASB has received a copy of the CRRESPRO model and integrated it in `UNIRAD`.

In Chapter 1 we describe the content and format of the CRRESPRO model. Chapter 2 reviews the way in which we adapted CRRESPRO to the AP-8 model data format for inclusion in `TREP`. The new version of `TREP` was tested on three standard orbits. In Chapter 3, the results of the flux predictions are compared to results obtained by Phillips Lab and to the fluxes predicted with AP-8 MAX.

Chapter 1

Description of CRRESPRO

The CRRESPRO software (Meffert & Gussenhoven 1994) uses flux models created from data collected by the proton telescope (PROTEL) on board the Combined Release and Radiation Effects Satellite (CRRES) flown from 25 July 1990 to 12 October 1991 during solar maximum (for a detailed description of the CRRES mission and the PROTEL instrument, see Violet et al. 1993, Heynderickx & Lemaire 1992). CRRES was in a geosynchronous transfer orbit with an inclination of 18°, a perigee of 350 km, and an apogee of 33 000 km. It traversed the radiation belts twice per orbit with a period of $9^{\mathrm{h}}52^{\mathrm{m}}$.

In March 1991, a magnetic storm caused a reconfiguration of the inner magnetosphere, resulting in, among other features, the formation of a second proton belt over a certain energy range. Because of this change, two CRRES models were created. The "quiet" model uses data from July 1990 to March 1991, and the "active" model uses data from March 1991 to October 1991. Note that the terms "quiet" and "active" have no correspondence to quiet and active as determined by the index K_{p}.

1.1 Flux models

The following description of the CRRESPRO models and data sets is taken from Meffert & Gussenhoven (1994).

The lower and upper boundaries and midpoint energies of PROTEL's 24 energy channels are given in Table 1. For each channel except channels 8 and 14 there are two data files, corresponding to quiet and active conditions, respectively.

The data files contain differential omnidirectional fluxes $j(E)$, where E is the midpoint energy for the corresponding channel. There are no files for channels 8 and 14.

Table 1. PROTEL energy channel parameters: lower, middle and higher energy

Channel	E_{lo}	E_{mid}	E_{hi}
1	1.0	1.5	2.1
2	2.0	2.1	2.3
3	2.2	2.5	2.8
4	2.8	2.9	3.2
5	3.1	3.6	4.1
6	3.9	4.3	4.8
7	4.6	5.7	7.0
8	7.3	8.4	9.4
9	6.0	6.8	7.7
10	7.5	8.5	9.6
11	9.3	9.7	10.2
12	9.9	10.7	11.5
13	11.2	13.2	15.2
14	14.7	15.2	15.9
15	15.5	16.9	18.3
16	18.0	19.4	20.8
17	25.3	26.3	27.2
18	26.1	30.9	35.6
19	34.9	36.3	37.7
20	37.8	41.1	48.1
21	44.3	47.0	53.5
22	53.3	55.0	62.1
23	62.1	65.7	73.1
24	73.1	81.3	100.0

The integral omnidirectional flux $J(> E)$ can be derived from the differential omnidirectional flux. Because of overlapping energy ranges, channels 5 and 15 were omitted from the integral omnidirectional flux calculation (in addition to channels 8 and 14 which are omitted from all calculations) and new boundaries were set up to prevent multiple contributions from the same energy. The energy bounds and widths of the remaining channels are shown in Table 2.

$J(> E_i)$ is defined as

$$J(> E_i) = \int_{E_i}^{\infty} j(E)\, dE\,, \tag{1.1}$$

where E_i is the lower energy boundary of channel i, as given in Table 2. The

Table 2. Integration parameters (MeV) for integral omnidirectional PROTEL flux

Channel	E_{lo}	E_{mid}	E_{hi}	ΔE
1	1.1	1.5	1.9	0.8
2	1.9	2.1	2.3	0.4
3	2.3	2.5	2.7	0.4
4	2.7	2.9	3.1	0.4
5	3.1	4.3	5.5	2.4
6	5.5	5.7	5.9	0.4
7	5.9	6.8	7.7	1.8
8	7.7	8.5	9.3	1.6
9	9.3	9.7	10.1	0.8
10	10.1	10.7	11.3	1.2
11	11.3	13.2	15.1	3.8
12	15.1	19.4	23.7	8.6
13	23.7	26.3	28.9	5.2
14	28.9	30.9	32.9	4.0
15	32.9	36.3	40.2	7.3
16	40.2	41.1	43.2	3.0
17	43.2	47.0	50.8	7.6
18	50.8	55.0	59.2	8.4
19	59.2	65.7	72.2	13.0
20	72.2	81.3	90.4	18.2

integration is approximated by a summation:

$$J(> E_i) = \sum_{k=i}^{20} j(E_k)\,\Delta E_k\,, \tag{1.2}$$

with ΔE_k the width of channel k. The integration summation for channel i begins at the lower boundary of that channel and ends at the new upper boundary of the highest energy channel, which is now channel 20 with an upper boundary of 90.4 MeV.

We have implemented only the integral omnidirectional flux model in `UNIRAD`, since this requires a significantly smaller modification of the `UNIRAD` software, as `TREP` is set up to read integral flux model data sets.

1.2 Model file format

The data files in the distribution of CRRESPRO consist of a set of files `FLUX_MOD.##`, where `##` ranges from `00` to `24`. The data files contain differential omnidirectional flux binned by L and B/B_0.

Each file starts with three header lines: a one-line title, a string containing the energy range, and a string containing the flux units. Each header line is a string of 136 eight bit characters. The first byte contains the number of characters in the string (0 to 136). The following bytes contain the characters in the string.

After the three header lines comes the data, consisting of a `REAL*4` array `D` of dimensions (90,34). The first index of `D` is associated with L and ranges from 1 to 90. The L bin limits are $(0.95 + 0.05i)\,R_E \leq L < (1.00 + 0.05i)\,R_E$. The second index of `D` is associated with B/B_0 and ranges from 1 to 34. The bin limits in B/B_0 are chosen so that each bin width corresponds to 2° in magnetic latitude and the total B/B_0 range approximately covers 68° magnetic latitude in a dipole field.

Chapter 2

Implementation in UNIRAD

In the UNIRAD software package, the routine TREP calculates integral and differential, omnidirectional or directional, proton and electron fluences for a given satellite orbit. To this effect, the (B, L) coordinates (McIlwain 1961) for each orbital point are determined and used as input to the NASA trapped radiation models AP-8 and AE-8 (Vette 1991b).

In order to incorporate the CRRESPRO quiet and active models into TREP, the model files have to be transformed into a block data format similar to the format of AP-8, as described by Vette (1991a). This transformation is described in the following sections.

2.1 Conversion of model files

The CRRESPRO software provided by Phillips Lab consists of a series of binary data files and executable program files, compiled for the IBM PC and compatibles. No source files or source listings are available.

From the description of the binary file format of the differential flux data files (Meffert & Gussenhoven 1994), we wrote a FORTRAN program to convert the binary data into ASCII format. These files contain the model data as twodimensional arrays of 90 L bins by 34 B/B_0 bins. The bin limits are $(0.95 + 0.05i)\,R_E \leq L < (1.00+0.05i)\,R_E$ in L, while the bin limits in B/B_0 are chosen so that each bin width corresponds to 2° in magnetic latitude and the total B/B_0 range approximately covers 68° magnetic latitude in a dipole field.

The NASA models AP-8 provide integral fluxes. Consequently, TREP expects integral fluxes from the model files it accesses. In order to keep the modifications to TREP to a minimum, we decided to produce two block data files, containing the CRRESPRO quiet and active integral fluxes, respectively. The ASCII files

obtained as described above were combined using Eq. (1.2) to form 40 new ASCII files containing the resulting values for $L, B/B_0, J(> E)$ for the integral channels in Table 2.

The AP-8 block data format stores, for each energy in the model and for each L value in the energy blocks, the logarithm of the equatorial integral flux and a series of increments in B/B_0 corresponding to a constant decrement in $\log J(> E)$. In contrast, the CRRESPRO model format gives the integral flux for a series of fixed values of B/B_0. In order to transform the CRRESPRO format into the AP-8 format, it is necessary to represent the dependence of the integral flux on B/B_0 by analytic functions. For the differential flux, Gussenhoven et al. (1993) considered a function of the form

$$j(E, \alpha_0) = j(E, 90°) \sin^n \alpha_0 \,, \tag{2.1}$$

where the equatorial pitch angle α_0 is defined as

$$\alpha_0 = \arcsin \sqrt{\frac{B_0}{B}} \tag{2.2}$$

and

$$B_0 = \frac{0.311653}{L^3} \,. \tag{2.3}$$

The values of the power index n were determined by least squares fitting to the model data.

A similar procedure can be followed for the integral flux $J(> E)$. Equation (2.1) is equivalent to

$$j(E, B/B_0) = j(E, 1) \left(\frac{B_0}{B}\right)^{n/2} \,. \tag{2.4}$$

Correspondingly, the integral flux may be written as

$$J(> E, B/B_0) = J(> E, 1) \left(\frac{B_0}{B}\right)^{n/2} \,. \tag{2.5}$$

For each of the channels listed in Table 2, we determined n by a least squares fit for every L value in the model files, both for the quiet and active models. As did Gussenhoven et al. (1993), we excluded the flux values in the two lowest pitch angle bins. The resulting values for n are plotted in Figs. 1 and 2 as a function of L for the quiet and active models, respectively. Figures 3 and 4 show the dependence on L of the equatorial integral flux $J(> E, 1)$ for the quiet and active models, respectively.

In order to obtain the same format as the AP-8 trapped particle models, we inverted Eq. (2.5) to the form

$$\left(\frac{B}{B_0}\right)_i = \left\{\frac{J(> E, 1)}{J[> E, (B/B_0)_i]}\right\}^{2/n} \,. \tag{2.6}$$

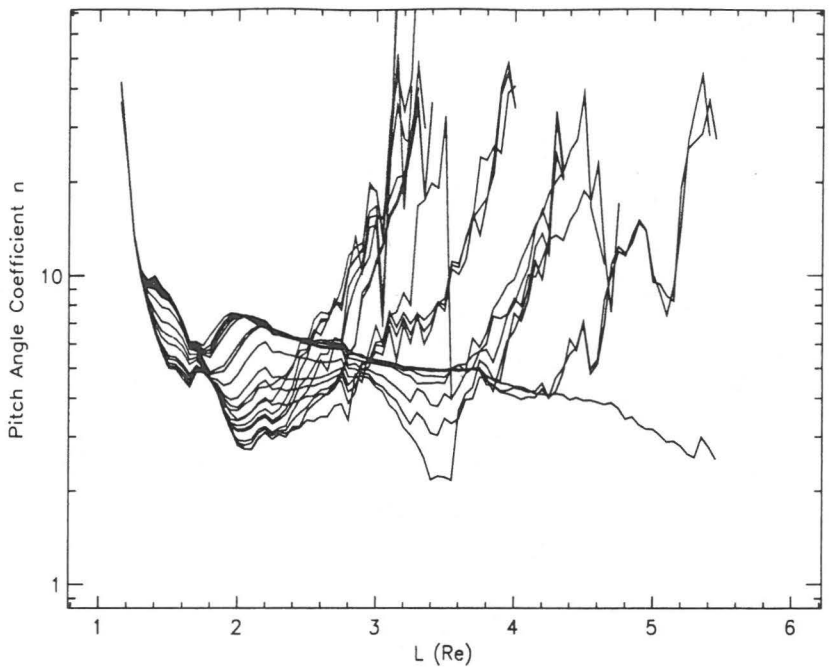

Figure 1. Power index of the fits of the integral flux distributions $J(> E, B/B_0)$ as a function of L, for the 20 CRRESPRO quiet models

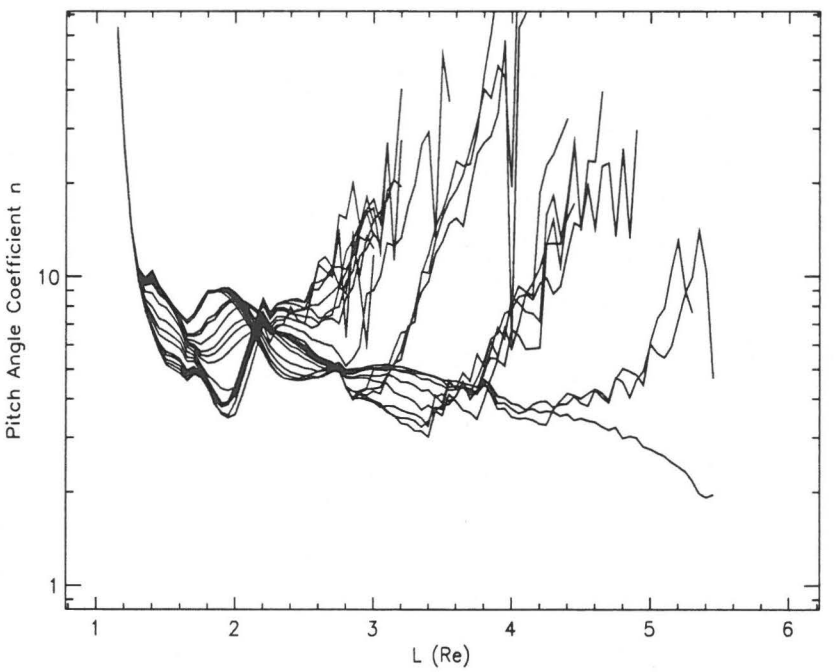

Figure 2. Power index of the fits of the integral flux distributions $J(> E, B/B_0)$ as a function of L, for the 20 CRRESPRO active models

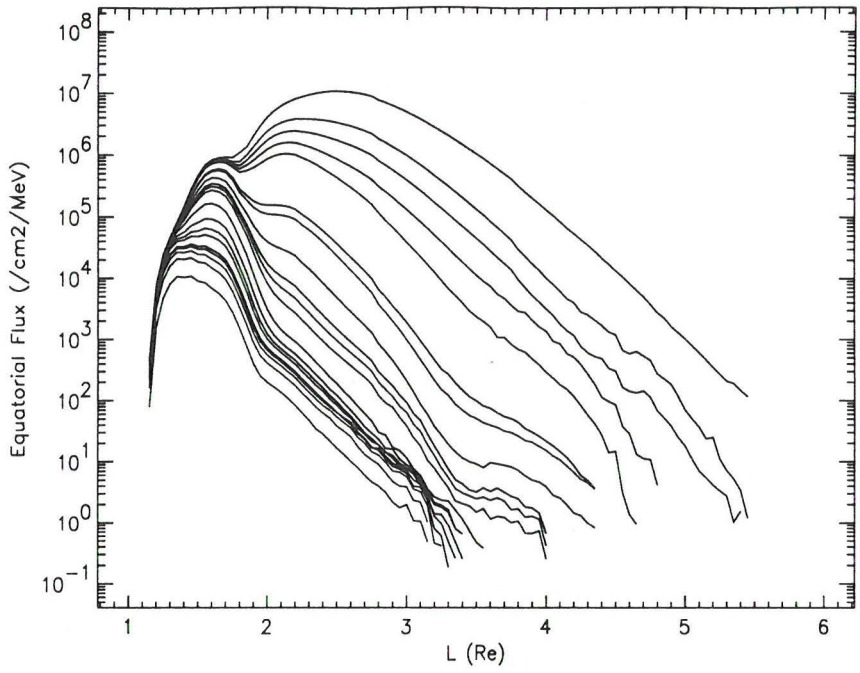

Figure 3. Equatorial integral flux as a function of L, for the 20 CRRESPRO quiet models

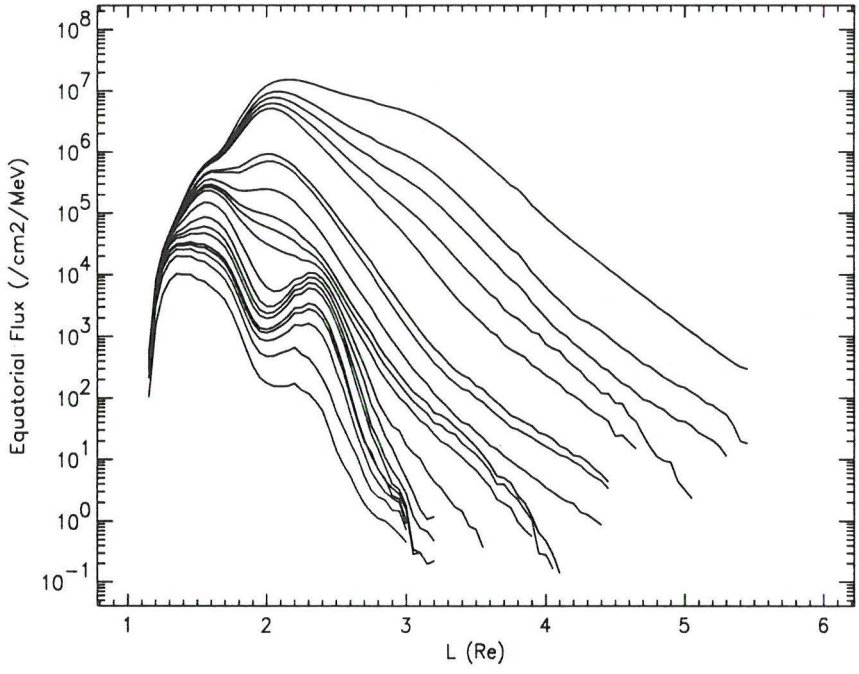

Figure 4. Equatorial integral flux as a function of L, for the 20 CRRESPRO active models

In AP-8, the decrement $\Delta \log J(> E) = 0.25$, i.e.

$$\frac{J[> E, (B/B_0)_i]}{J(> E, 1)} = 10^{-0.25i} . \tag{2.7}$$

With Eq. (2.6), the corresponding $(B/B_0)_i$ values are derived:

$$\left(\frac{B}{B_0}\right)_i = 10^{0.5i/n} . \tag{2.8}$$

The $\Delta(B/B_0)$ increments are given by

$$\Delta\left(\frac{B}{B_0}\right)_i = \left(\frac{B}{B_0}\right)_i - \left(\frac{B}{B_0}\right)_{i-1} . \tag{2.9}$$

Figures 5 and 6 show the $J(> E, \alpha_0)$ points in the original CRRESPRO quiet and active model files for two L values (1.6 and 2.2) and for four energies (4.3, 9.7, 26.3 and 55.0 MeV), overlaid with curves representing the fitted flux dependence [a similar figure is given by Gussenhoven et al. (1993)]. For $L = 1.6$, the fitted fluxes represent the model data well, except near the loss cone where the fit function does not fall off as the model data does. This effect is due on the one hand to the non-inclusion of the last two model points in the fitting procedure and on the other hand to the failure of a function of the form of Eq. (2.5) to fit the pitch angle range from equator to loss cone. As a consequence, the flux predicted with the fitted functions may be overestimated near the loss cone.

For higher L values, e.g. $L = 2.2$ (Fig. 6), the situation is somewhat different. For the lowest energies, the fit functions represent the model flux well. However, for $E > 10$ MeV the model flux does not decrease monotonically towards the loss cone, but reaches a plateau first. Gussenhoven et al. (1993) attributed this to the existence of two populations of trapped protons. Obviously, a single fit function is not sufficient to describe the pitch angle dependence of the sum of two populations, which leads to an underestimate of the fitted flux near the equator and a possible overestimate near the loss cone.

The limitations of the fitting procedure also are apparent in Figs. 1 and 2, in that the dependence of n on L is somewhat erratic. It would be better to access the CRRESPRO model data by direct interpolation between E, L and B/B_0 values instead of using a fitted dependence of the flux on B/B_0. However, this procedure requires major modifications of `TREP`, which are beyond the scope of this study.

The fitting of the model fluxes could be improved in two ways. Firstly, a sum of two functions of the form of Eq. (2.5) could be fitted to the model fluxes instead of just a single function. Secondly, a different fit function could be used, e.g. the function proposed by Badhwar & Konradi (1990), which has been applied to the AP-8 flux distribution by Heynderickx & Lemaire (1993). This improvement may be a topic in a follow-on TREND study.

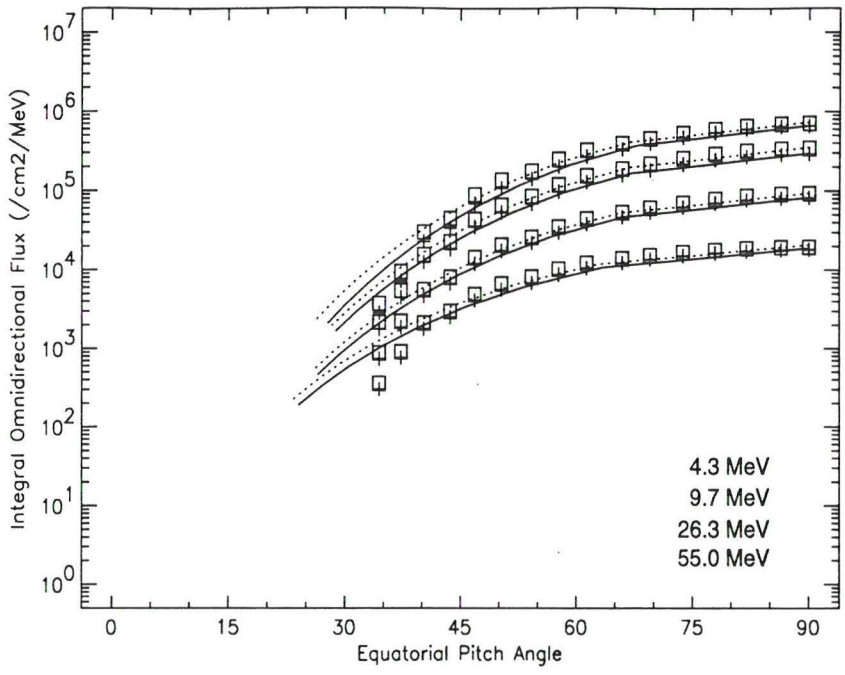

Figure 5. $J(> E, \alpha_0)$ for four energies and $L = 1.6$. The symbols □ and + denote the quiet and active values, respectively, in the original model data files, the dotted and solid lines represent the fitted quiet and active fluxes, respectively.

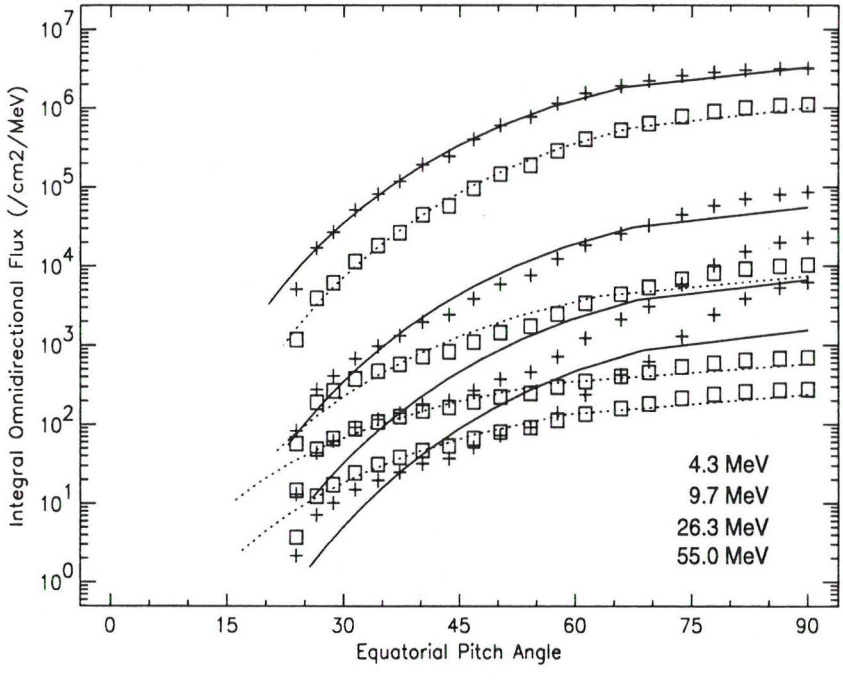

Figure 6. $J(> E, \alpha_0)$ for four energies and $L = 2.2$. The symbols and lines have the same meaning as in Fig. 5.

2.2 Implementation in TREP

The $\Delta(B/B_0)$ increments for each energy and L value in the CRRESPRO models were then stored in the `BLOCK DATA` format of the AP-8 models (Vette 1991a), in the files `CRRQUI.FOR` and `CRRACT.FOR`, corresponding to the quiet and active model, respectively. The `NAMELIST` for `TREP` was extended to make use of the newly added models.

The parameter `TRPMOD` chooses between the NASA proton and electron models AP-8 and AE-8 on the one hand, and the proton and electron models based on CRRES data on the other hand. The CRRES based electron models were generated at MSSL (Rodgers 1994). `CRRACT` chooses between the quiet and the active CRRESPRO models. A table with the `NAMELIST` parameters for `TREP` can be found in the `UNIRAD` user manual.

Chapter 3

Application to standard orbits

In this chapter we apply the CRRESPRO models, as we implemented them in TREP, to three standard orbits: a geostationary transfer orbit (GTO), a low-Earth orbit (LEO), and a polar orbit.

3.1 Geostationary transfer orbit

The CRRESPRO documentation (Meffert & Gussenhoven 1994) contains a sample run of the software for a typical CRRES orbit. The integral omnidirectional fluence over this orbit is listed in Table 3.

Using TREP, we have calculated the fluence over one day accumulated along a trajectory (represented in Fig. 7) with the same orbital parameters, with the newly implemented CRRESPRO models and with AP-8 MAX. For CRRESPRO we used the IGRF 90 magnetic field model, updated to 1991.0, and the Olson & Pfitzer (1977) quiet external field model. For AP-8 MAX we used the GSFC 12/66 model (Cain et al. 1967), updated to 1970, and corrected for the westward drift of the SAA. The resulting fluxes and the flux spectrum are represented graphically in Figs. 8 to 13. The fluences for one orbit are listed in Table 3.

From the table and the figures it can be seen that the differences between the quiet and active CRRESPRO fluences are small for this orbit, i.e. at most about a factor two. The fluences calculated with the CRRESPRO models implemented in TREP are within a factor of two of the fluences obtained by Meffert & Gussenhoven (1994) with the original CRRESPRO model. The causes of this difference have been discussed in Sect. 2.1. The fluences obtained with AP-8 MAX are up to a factor two larger than the fluences obtained with CRRESPRO, both the active and quiet version.

As a further comparison, we show in Figs. 14 and 15 the Science Summary

Table 3. Integral omnidirectional fluence $J(> E)$ in $\mathrm{cm}^{-2}\mathrm{year}^{-1}$ for a typical CRRES orbit. The first column gives the energy E, the second and fourth column contain the fluences obtained with the extended version of TREP, using the quiet and active CRRESPRO models, respectively. The third and fifth columns give the fluences listed by Meffert & Gussenhoven (1994). The sixth column contains the fluences obtained with AP-8 MAX.

E (MeV)	J_{qTREP}	J_{qMG}	J_{aTREP}	J_{aMG}	$J_{\mathrm{AP-8\,MAX}}$
1.1	1.29×10^{13}	1.85×10^{13}	1.69×10^{13}	2.26×10^{13}	5.12×10^{13}
1.9	4.27×10^{12}	5.68×10^{12}	7.52×10^{12}	9.32×10^{12}	1.23×10^{13}
2.3	2.55×10^{12}	3.20×10^{12}	5.23×10^{12}	6.31×10^{12}	8.07×10^{12}
2.7	1.61×10^{12}	1.87×10^{12}	3.77×10^{12}	4.45×10^{12}	5.76×10^{12}
3.1	1.10×10^{12}	1.19×10^{12}	2.83×10^{12}	3.30×10^{12}	4.26×10^{12}
5.5	4.24×10^{11}	3.53×10^{11}	7.19×10^{11}	7.51×10^{11}	1.28×10^{12}
5.9	3.76×10^{11}	3.03×10^{10}	5.96×10^{11}	6.11×10^{11}	1.10×10^{12}
7.7	2.60×10^{11}	1.95×10^{11}	3.23×10^{11}	2.94×10^{11}	6.17×10^{11}
9.3	2.03×10^{11}	1.46×10^{11}	2.18×10^{11}	1.78×10^{11}	3.97×10^{11}
10.1	1.83×10^{11}	1.30×10^{11}	1.88×10^{11}	1.47×10^{11}	3.23×10^{11}
11.3	1.59×10^{11}	1.12×10^{11}	1.56×10^{11}	1.17×10^{11}	2.50×10^{11}
15.1	1.05×10^{11}	7.22×10^{10}	9.97×10^{10}	7.13×10^{10}	1.16×10^{11}
23.7	6.75×10^{10}	4.60×10^{10}	6.44×10^{10}	4.65×10^{10}	5.00×10^{10}
28.9	5.10×10^{10}	3.47×10^{10}	4.95×10^{10}	3.58×10^{10}	3.65×10^{10}
32.9	4.23×10^{10}	2.89×10^{10}	4.11×10^{10}	2.98×10^{10}	3.17×10^{10}
40.2	3.03×10^{10}	2.07×10^{10}	2.93×10^{10}	2.09×10^{10}	2.63×10^{10}
43.2	2.78×10^{10}	1.90×10^{10}	2.67×10^{10}	1.89×10^{10}	2.44×10^{10}
50.8	2.32×10^{10}	1.59×10^{10}	2.20×10^{10}	1.54×10^{10}	2.05×10^{10}
59.2	1.74×10^{10}	1.19×10^{10}	1.63×10^{10}	1.11×10^{10}	1.81×10^{10}
72.2	8.55×10^{9}	5.84×10^{9}	8.00×10^{9}	5.40×10^{9}	1.52×10^{10}

Data Base (SSDB) PROTEL HEH-13 flux for orbit 703—which corresponds to the sample orbit in this section—and the proton flux for the same orbit obtained with AP-8 MAX and the quiet and active CRRESPRO models. It can be seen that the model fluxes are higher than the observed fluxes by about a factor of two. As expected, the secondary radiation belt visible in the SSDB flux is present only in the active CRRESPRO results.

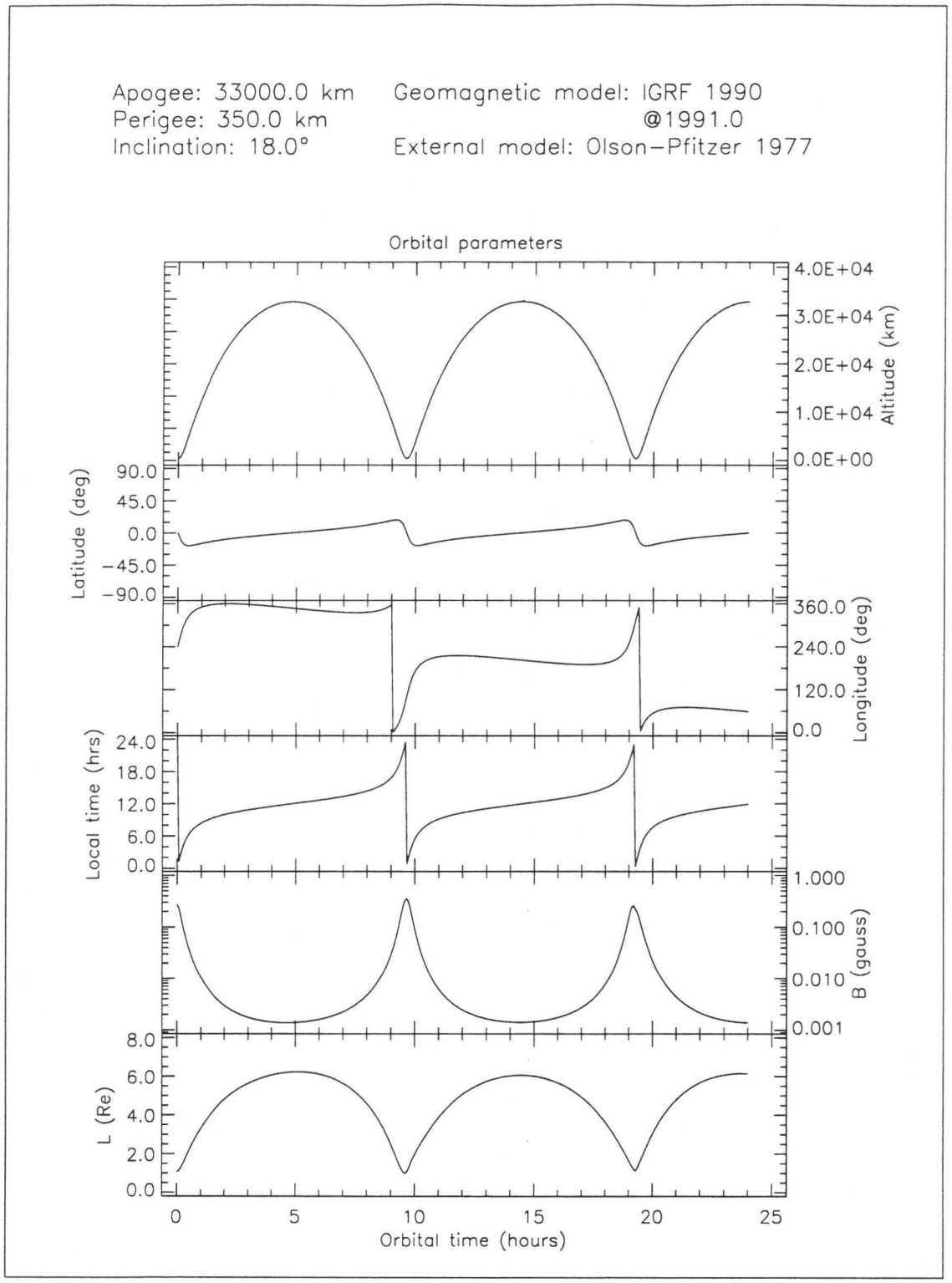

Figure 7. Geographic and magnetic coordinates for the sample CRRES orbit described in the text

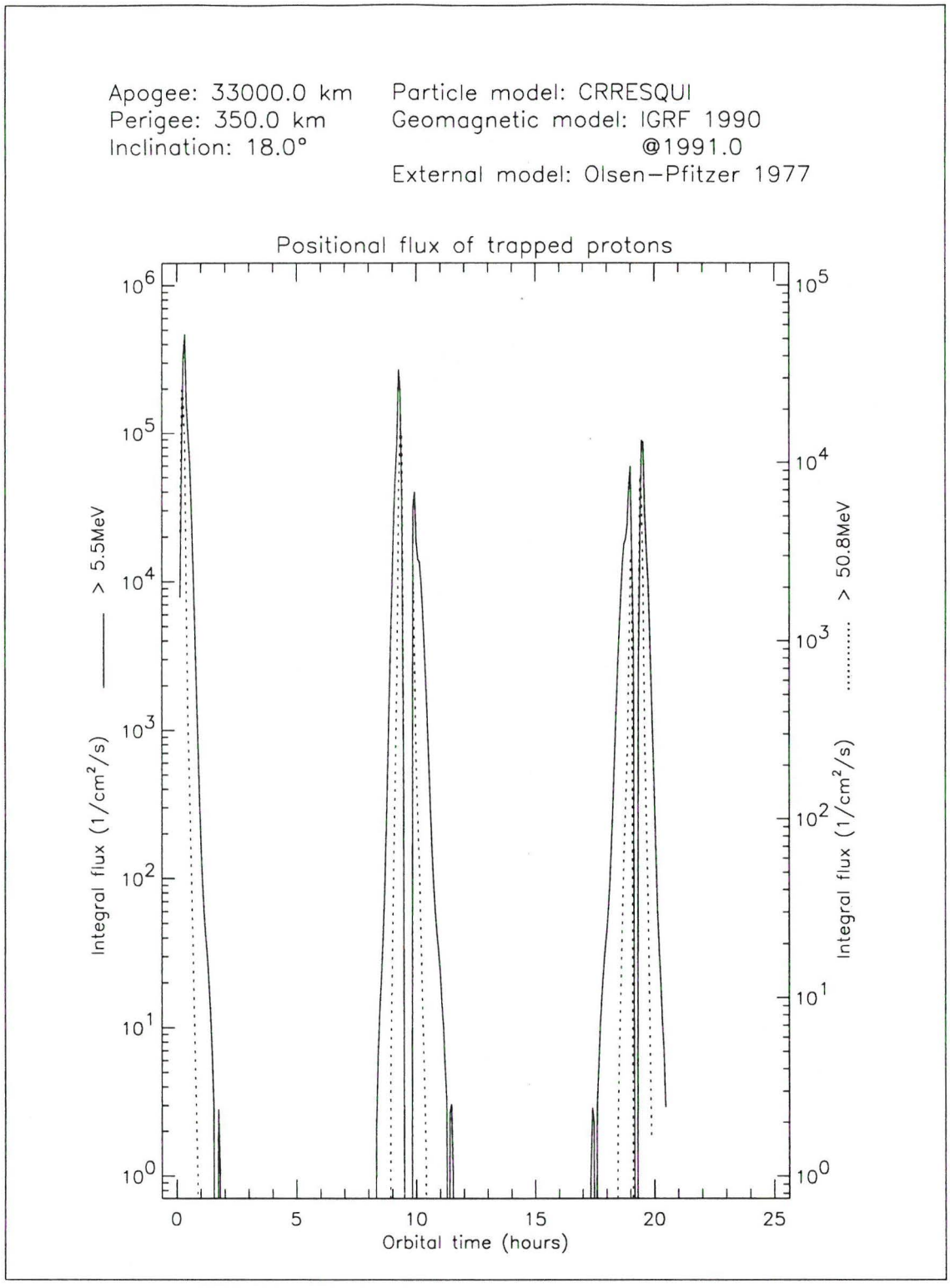

Figure 8. Differential CRRESPRO/QUIET proton flux along the sample CRRES orbit described in the text

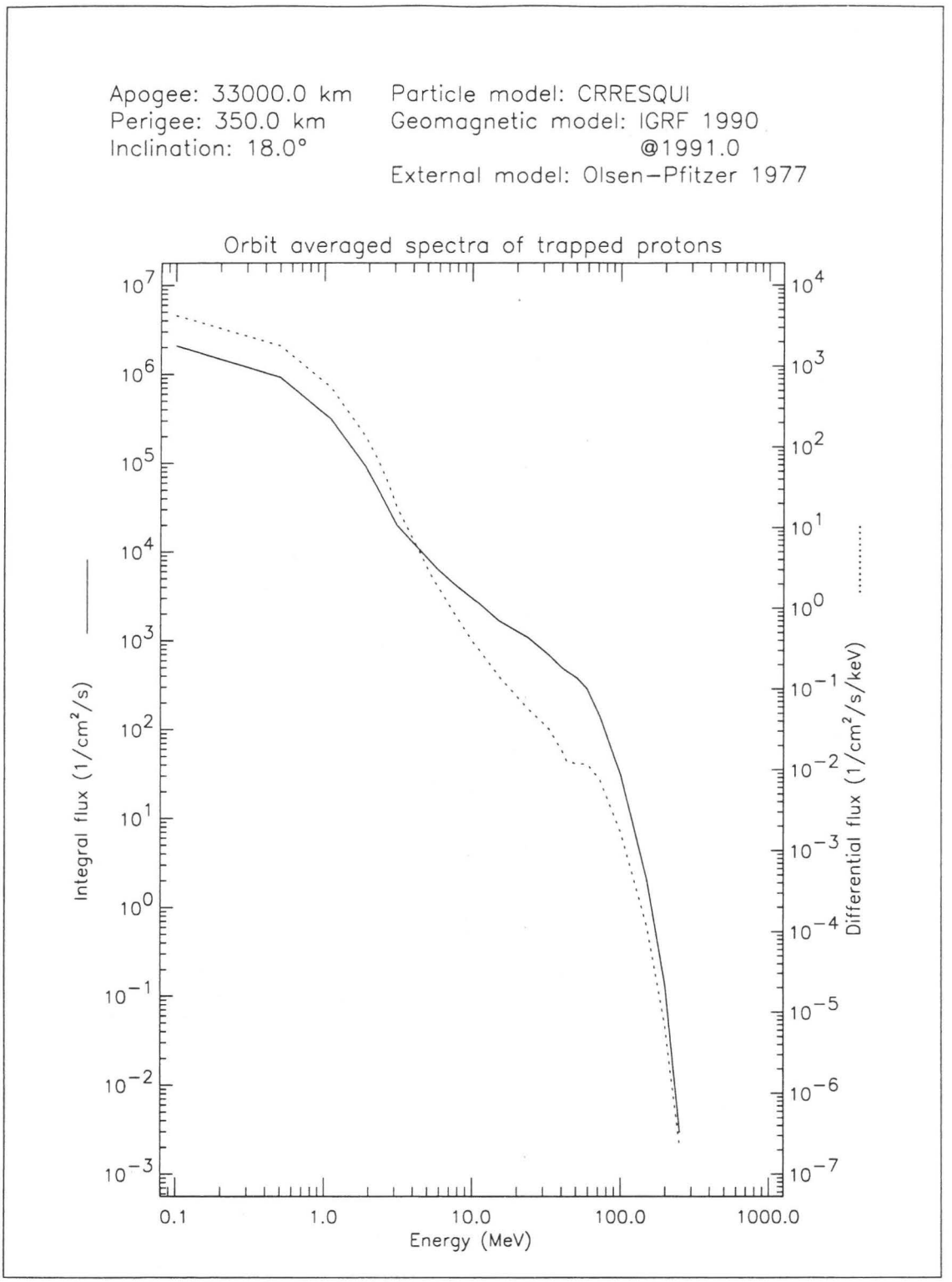

Figure 9. Integral and differential CRRESPRO/QUIET proton spectrum along the sample CRRES orbit described in the text

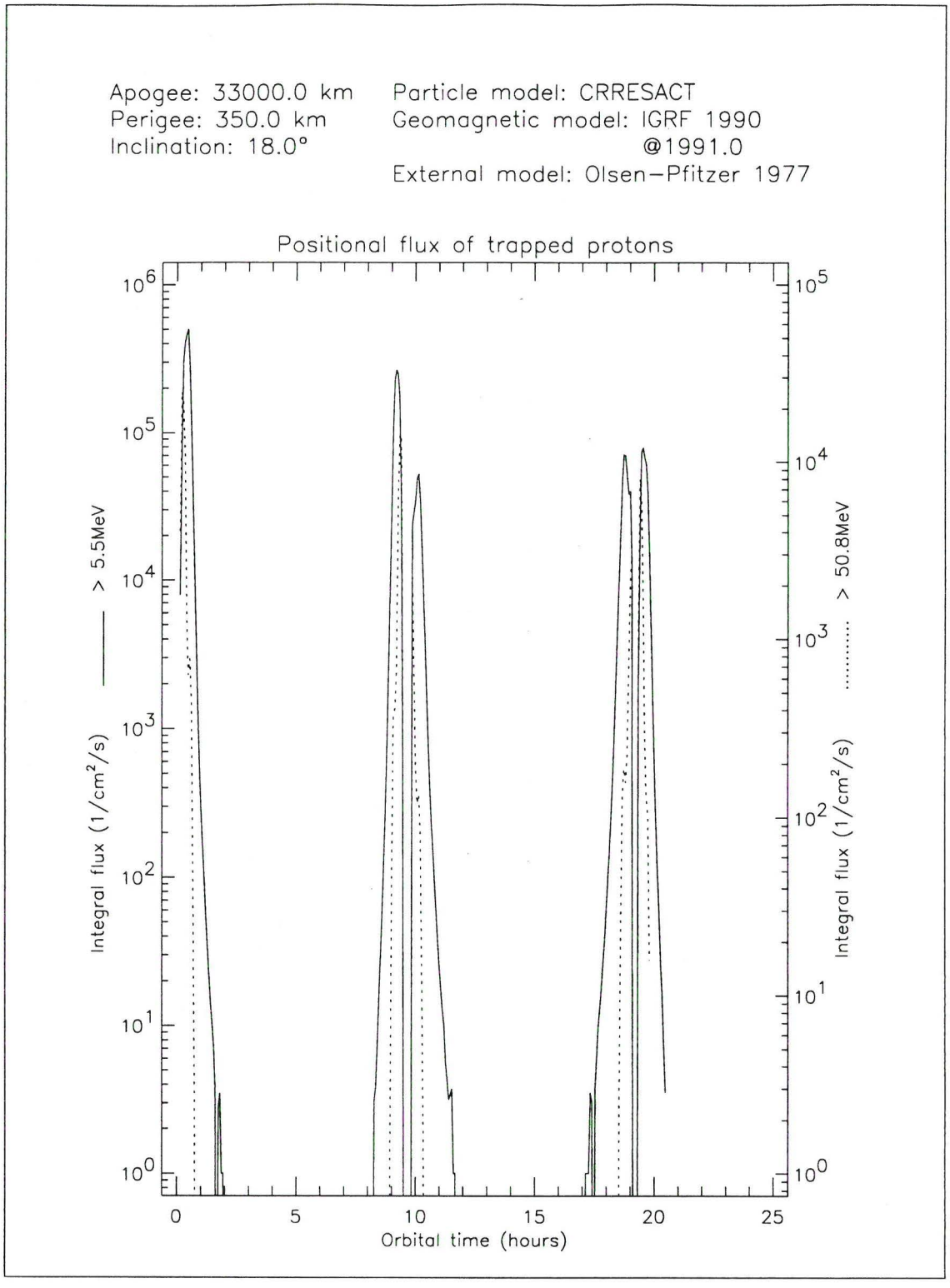

Figure 10. Differential CRRESPRO/ACTIVE proton flux along the sample CRRES orbit described in the text

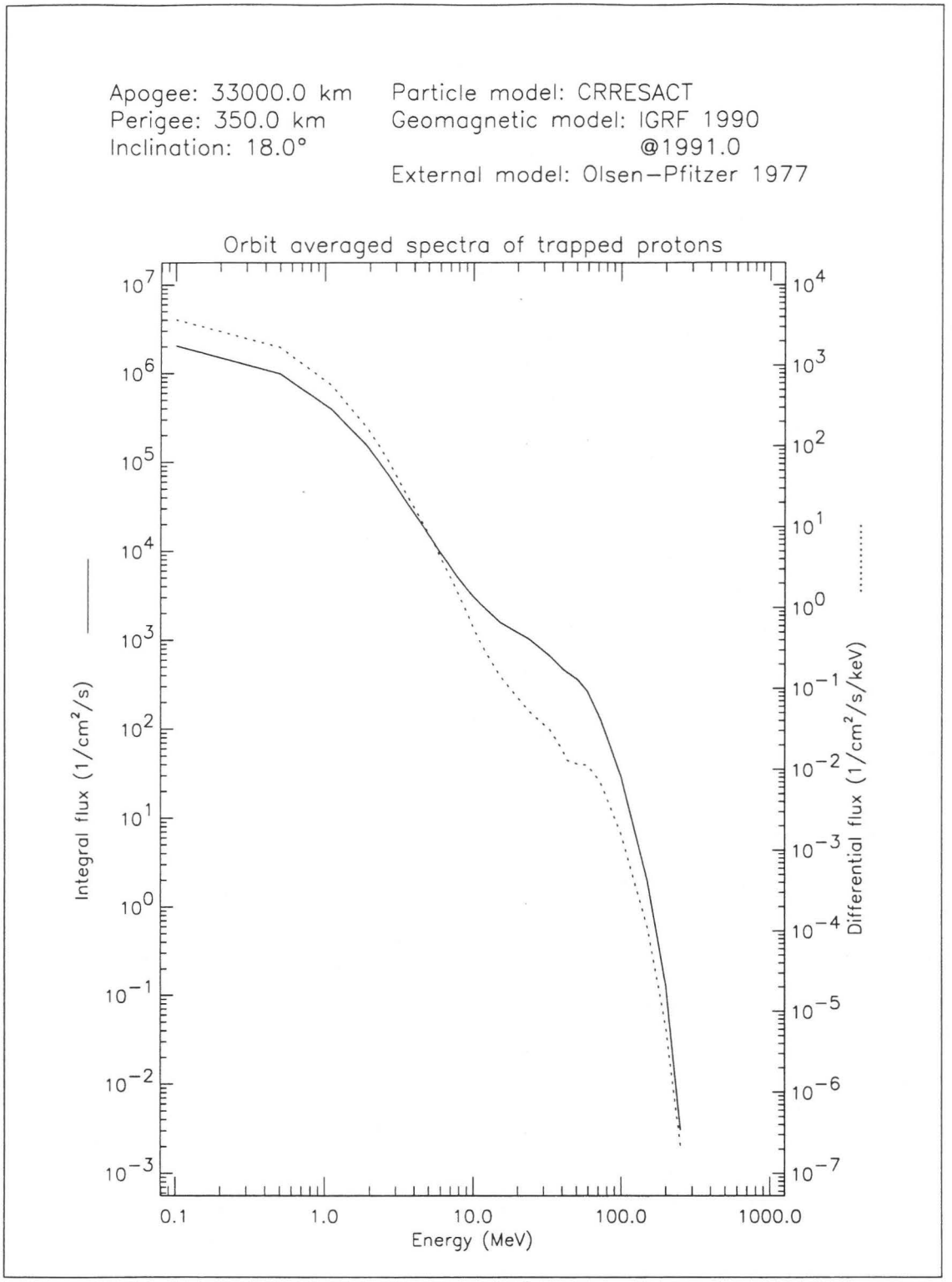

Figure 11. Integral and differential CRRESPRO/ACTIVE proton spectrum along the sample CRRES orbit described in the text

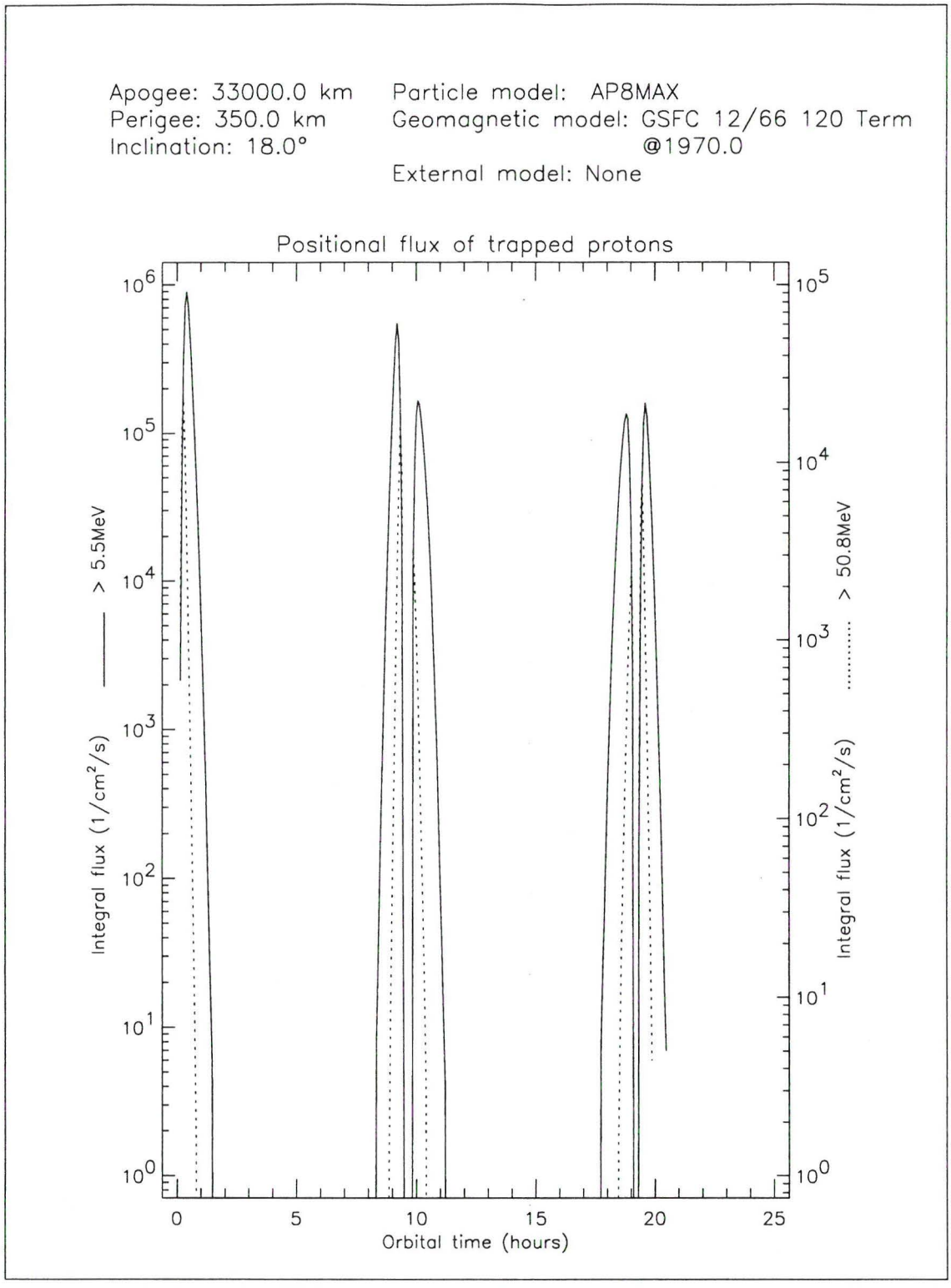

Figure 12. Differential AP-8 MAX proton flux along the sample CRRES orbit described in the text

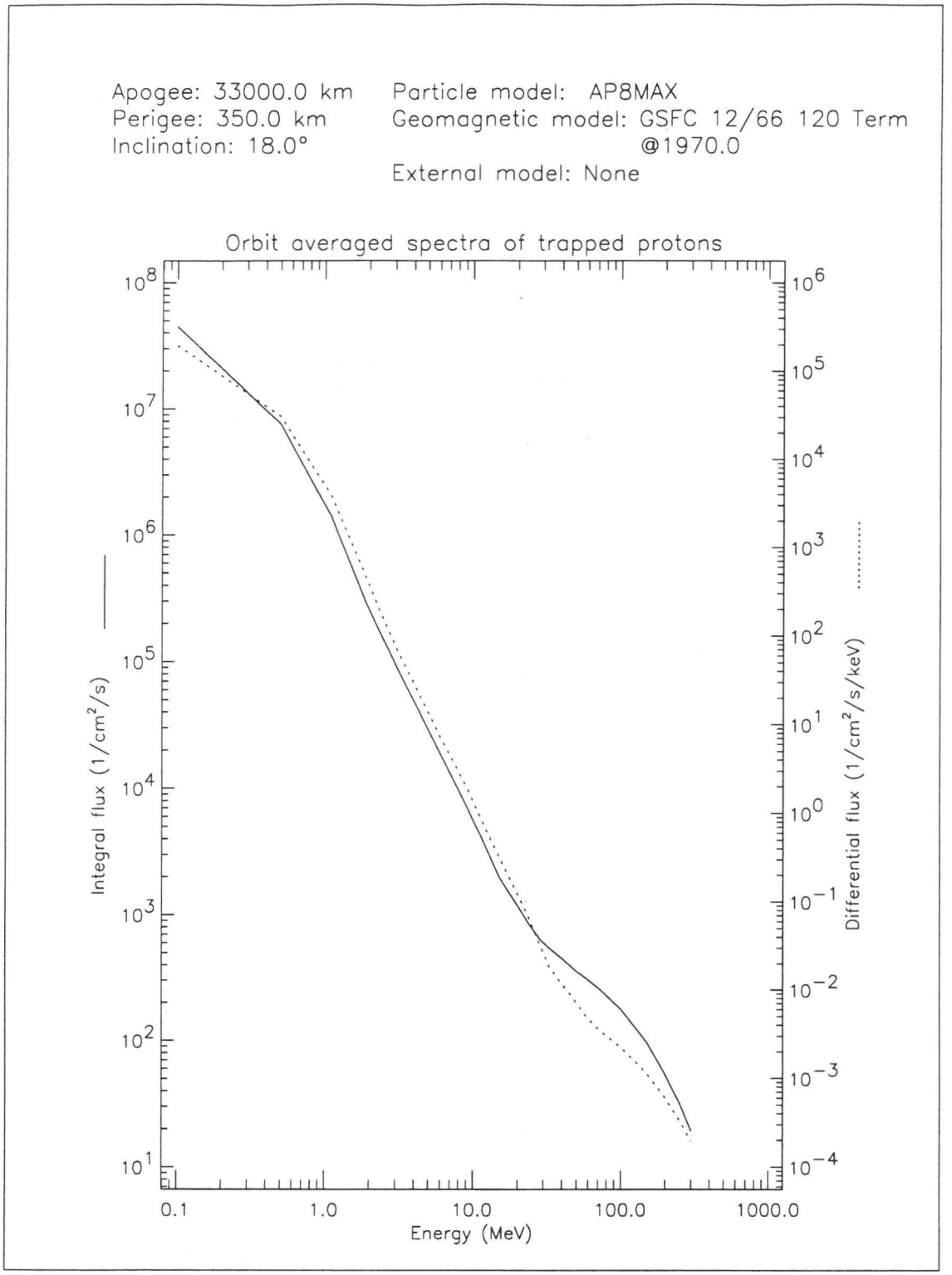

Figure 13. Integral and differential AP-8 MAX proton spectrum along the sample CRRES orbit described in the text

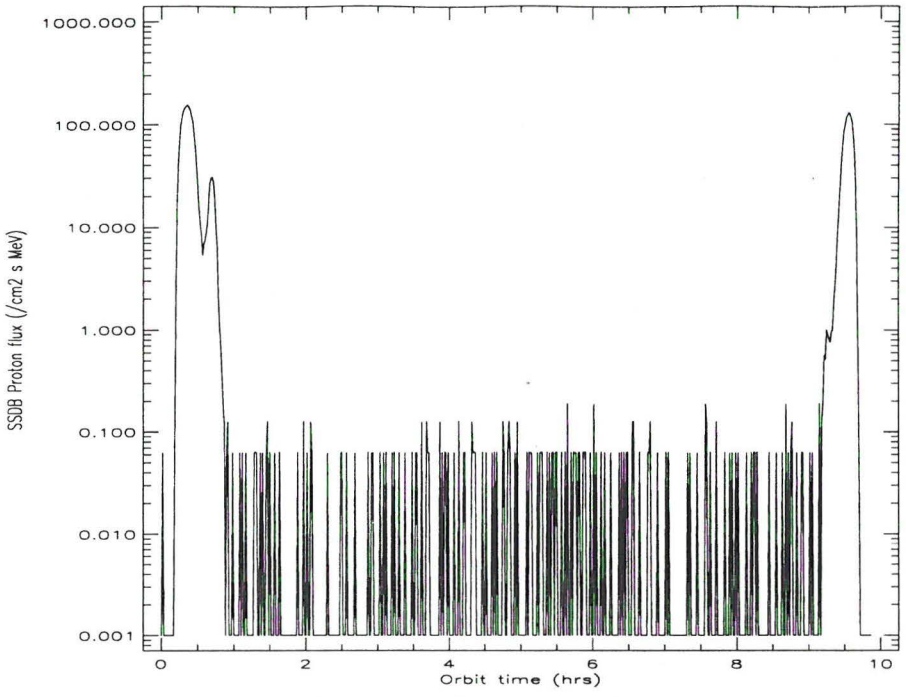

Figure 14. SSDB PROTEL HEH-13 proton flux for CRRES orbit 703

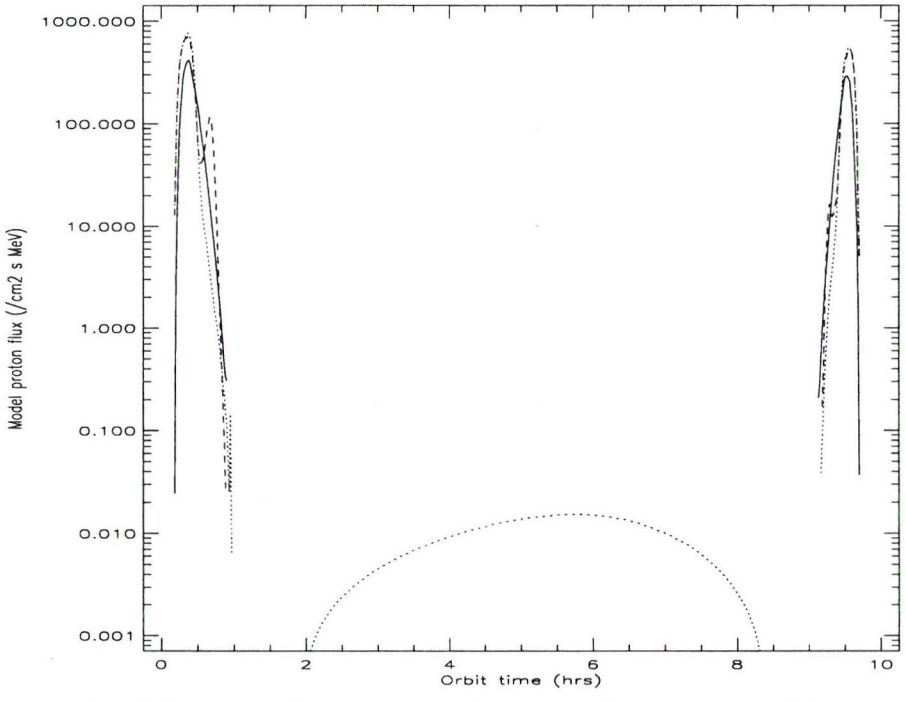

Figure 15. Model proton flux for CRRES orbit 703. The solid line represents the AP-8 MAX flux, the dotted line the CRRESPRO quiet flux and the dashed line the CRRESPRO active flux.

3.2 Low Earth orbit

The CRRESPRO model was also applied to a circular LEO orbit, represented in Fig. 16, with altitude 350 km and inclination 28.5°. The fluxes and flux spectra obtained with the quiet and active CRRESPRO models and with AP-8 MAX are represented in Figs. 17 to 22. For CRRESPRO we used the IGRF 90 magnetic field model, updated to 1991.0, and the Olson & Pfitzer (1977) quiet external field model. For AP-8 MAX we used the GSFC 12/66 model (Cain et al. 1967), updated to 1970, and corrected for the westward drift of the SAA.

The CRRESPRO quiet flux generally is about a factor of two higher than the CRRESPRO active flux. More strikingly, the AP-8 MAX positional flux is on average up to a factor of a hundred lower than the CRRESPRO flux! This discrepancy is undoubtedly due to the poor representation of the loss cone with the functions we used to fit the CRRESPRO model data. When comparing Figs. 17 and 19 to Fig. 21 it is clear that the AP-8 MAX flux is limited to five orbital passes over longitudes corresponding to the location of the South Atlantic Anomaly (SAA), while the CRRESPRO model predicts significant fluxes for almost every orbit. This also explains why the AP-8 MAX fluence spectrum (Fig. 22) is so much lower than the CRRESPRO fluence spectra (Figs. 18 and 20).

3.3 Polar orbit

As a third test, we applied the CRRESPRO model to a circular polar orbit, represented in Fig. 23, with altitude 840 km and inclination 98.8°. The fluxes and flux spectra obtained with the quiet and active CRRESPRO models and with AP-8 MAX are represented in Figs. 24 to 29. For CRRESPRO we used the IGRF 90 magnetic field model, updated to 1991.0, and the Olson & Pfitzer (1977) quiet external field model. For AP-8 MAX we used the GSFC 12/66 model (Cain et al. 1967), updated to 1970, and corrected for the westward drift of the SAA.

As in the case of the LEO orbit, the CRRESPRO fluxes and fluences are much higher than the AP-8 MAX values, due to the overestimate by CRRESPRO of fluxes near the loss cone.

3.4 Conclusions

The fitting procedure we used to implement the CRRESPRO model in `TREP` is not satisfactory. Either an improved fit function [like that of Badhwar & Konradi (1990), or a sum of two functions] should be used or the same software used by CRRESPRO to access the data files should be implemented in `TREP`. This latter improvement

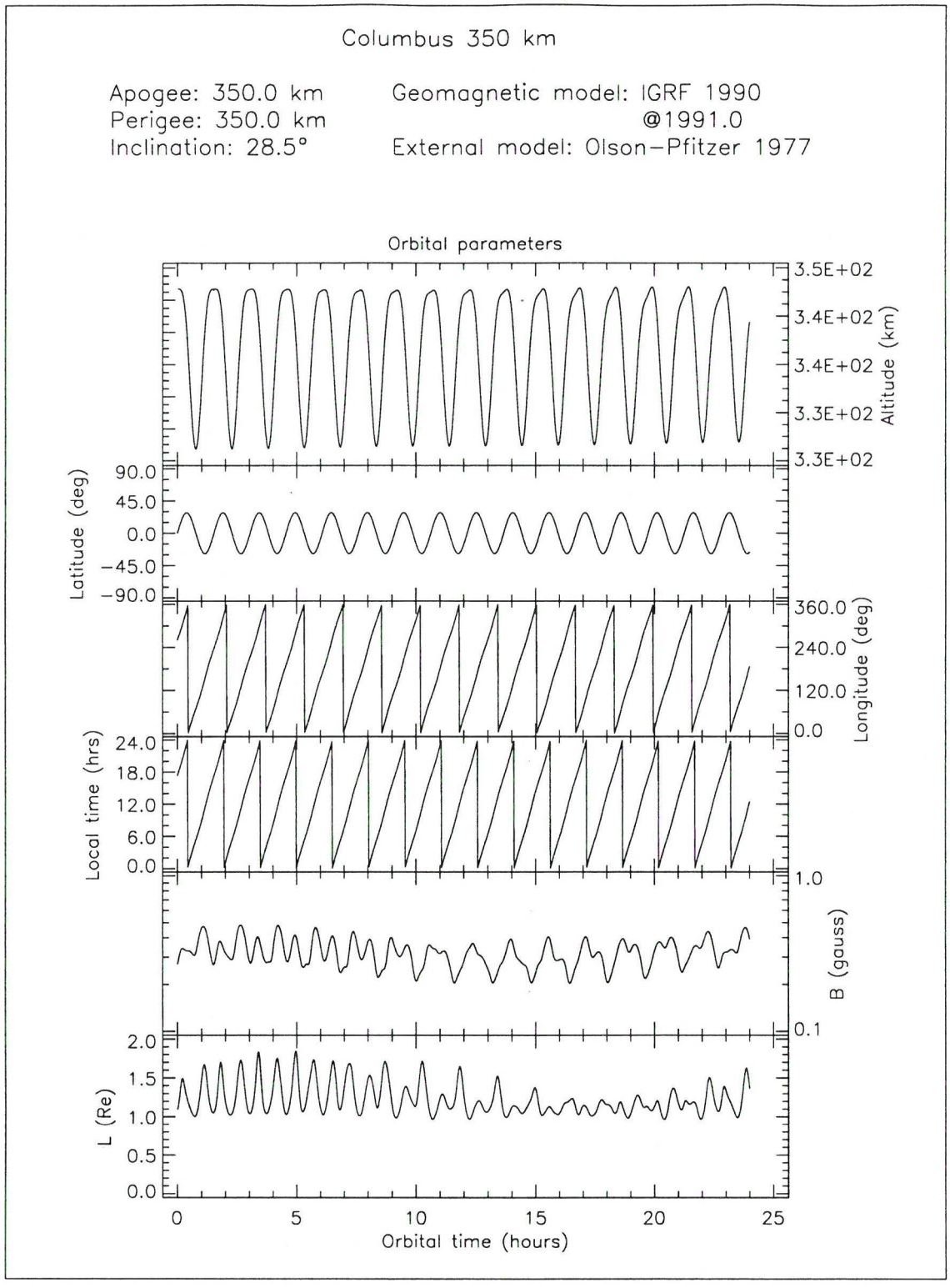

Figure 16. Geographic and magnetic coordinates for the LEO orbit described in the text

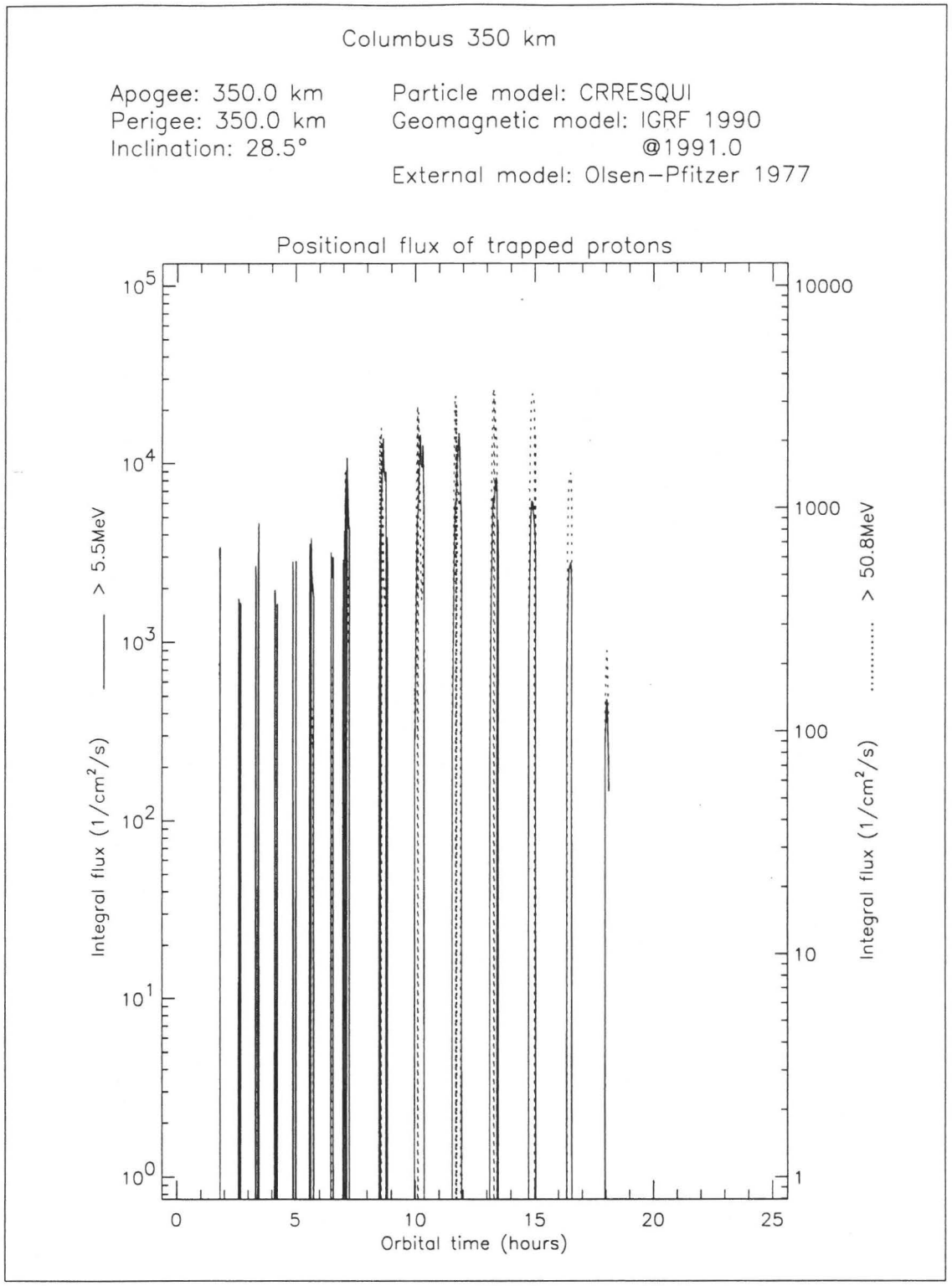

Figure 17. Differential CRRESPRO/QUIET proton flux along the LEO orbit described in the text

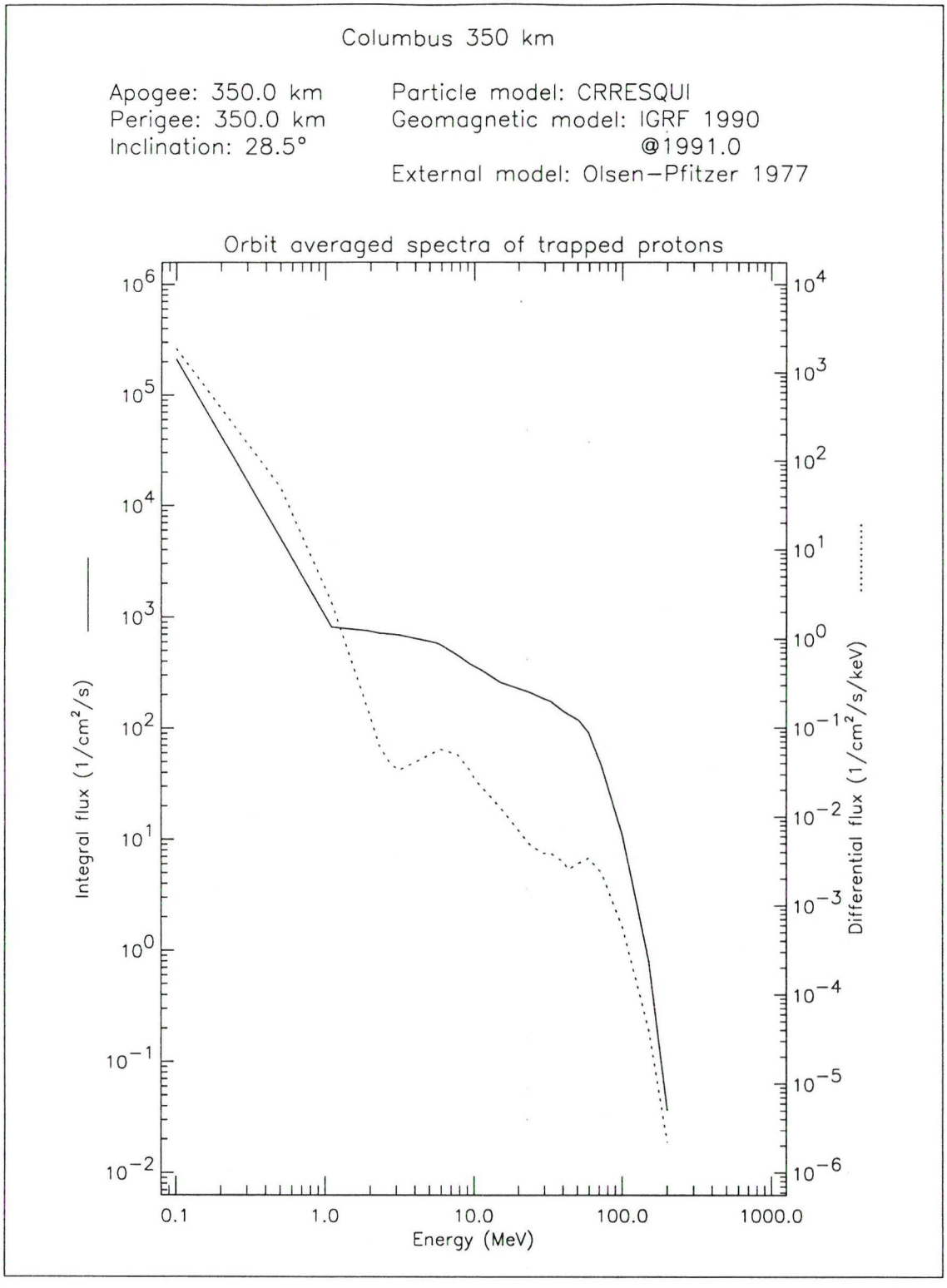

Figure 18. Integral and differential CRRESPRO/QUIET proton spectrum along the LEO orbit described in the text

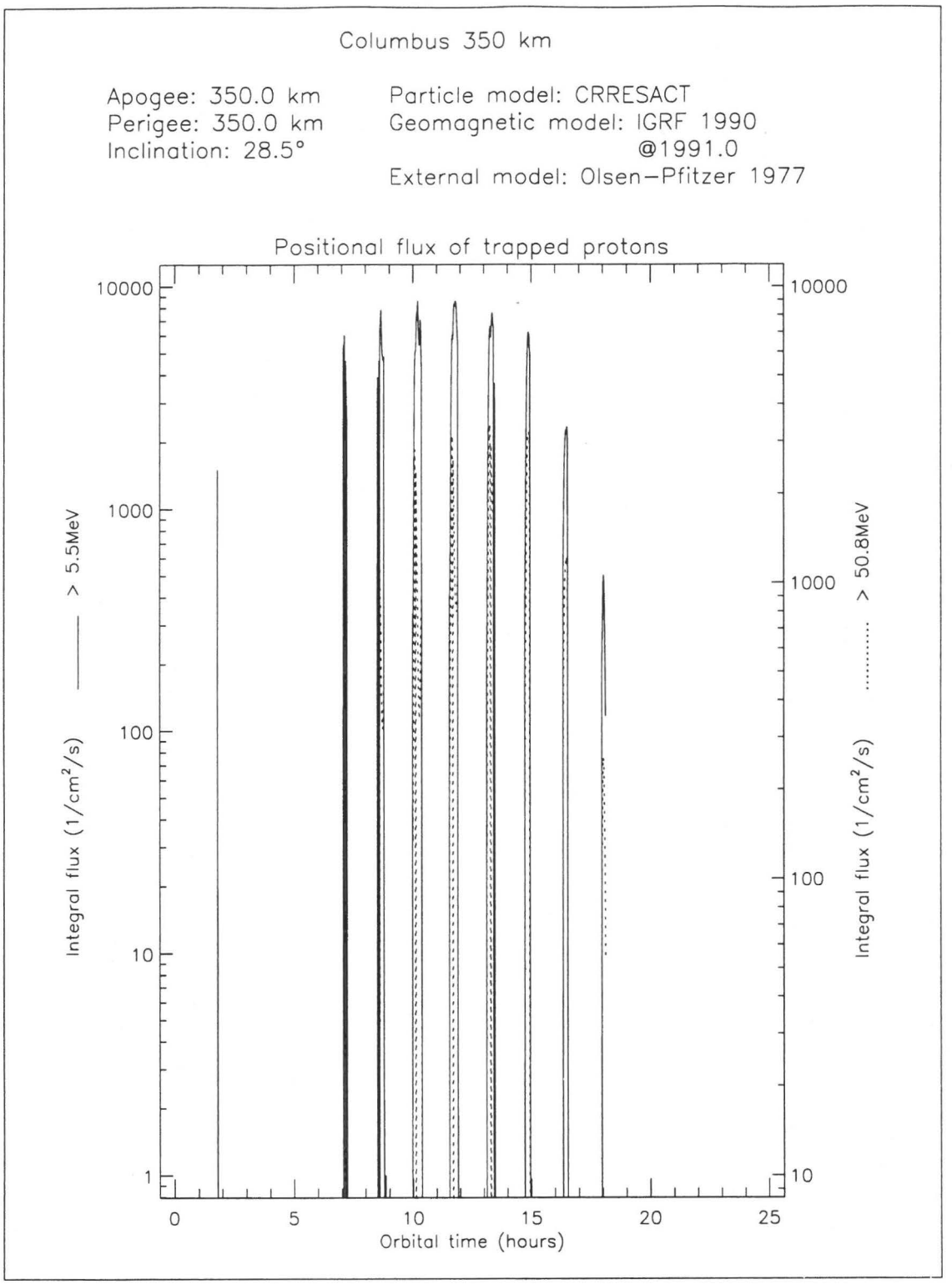

Figure 19. Differential CRRESPRO/ACTIVE proton flux along the LEO orbit described in the text

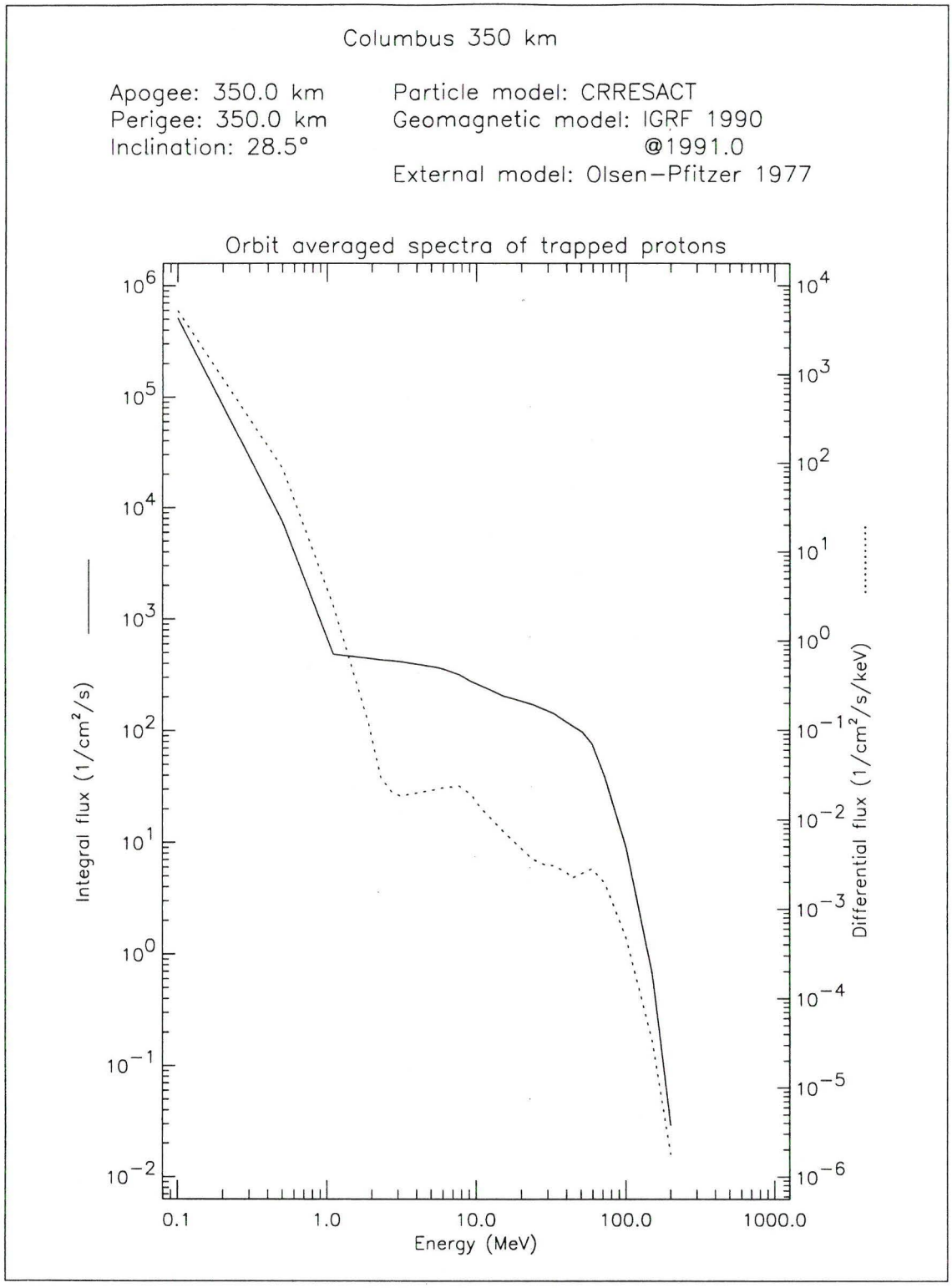

Figure 20. Integral and differential CRRESPRO/ACTIVE proton spectrum along the LEO orbit described in the text

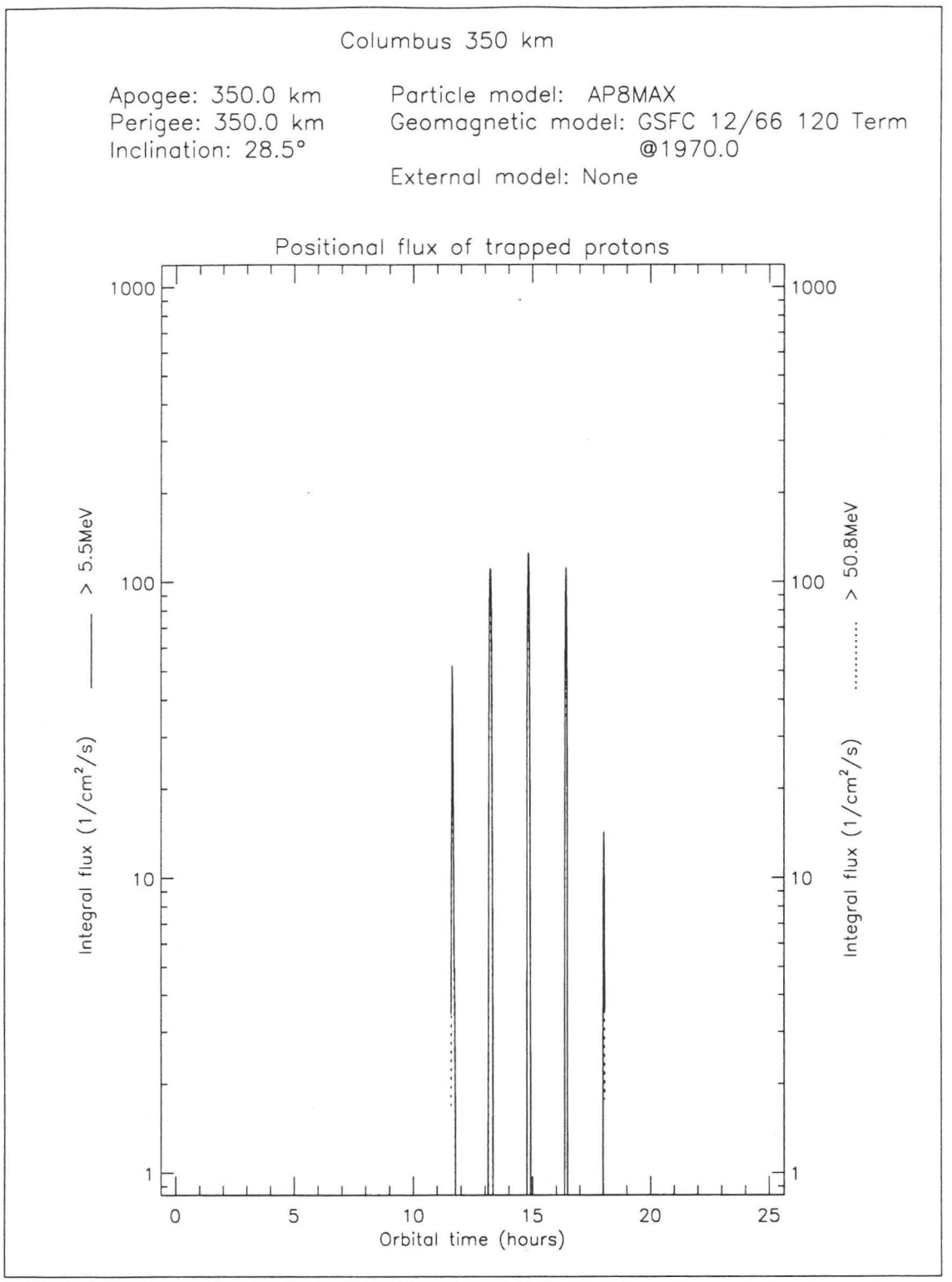

Figure 21. Differential AP-8 MAX proton flux along the LEO orbit described in the text

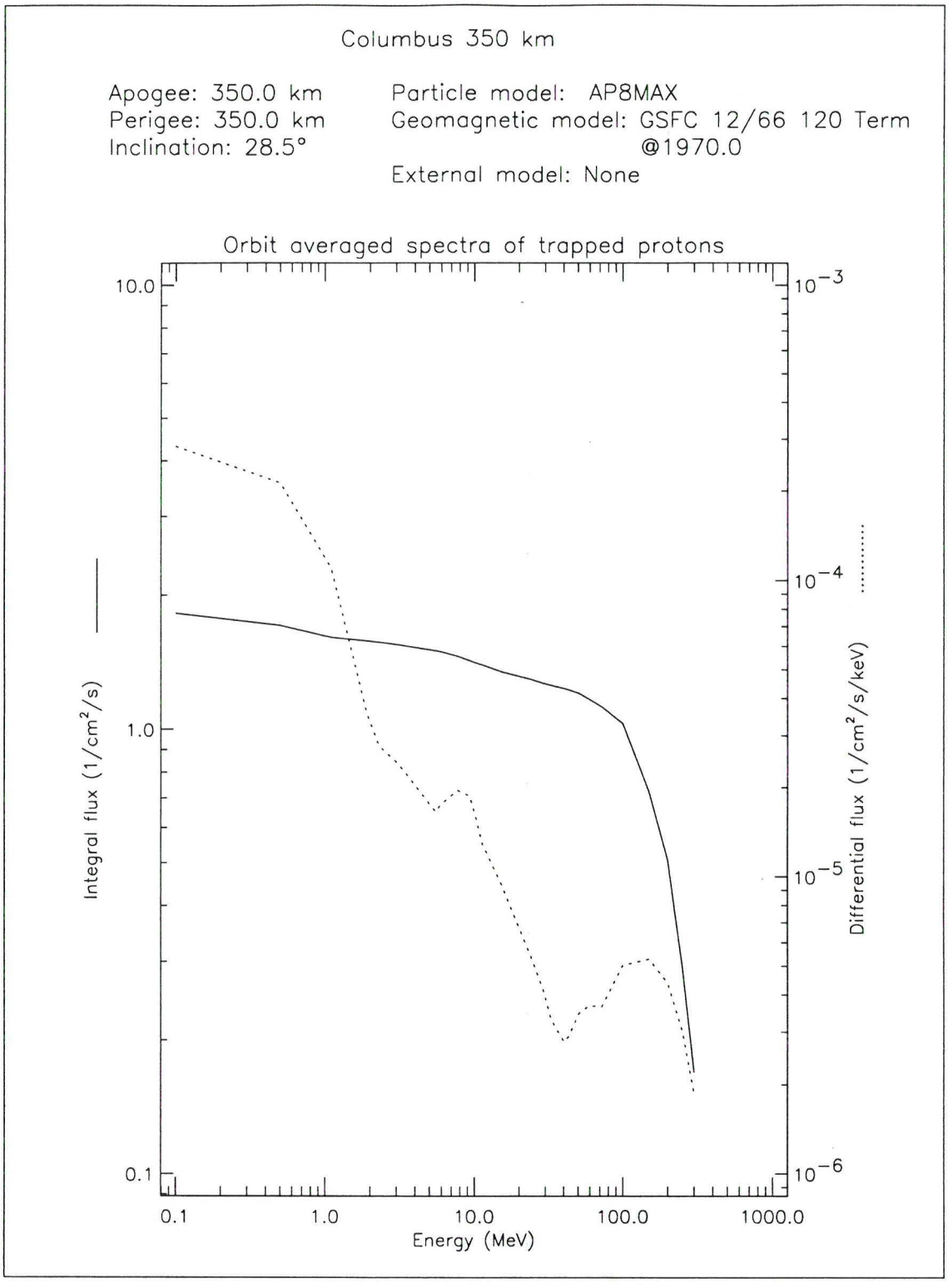

Figure 22. Integral and differential AP-8 MAX proton spectrum along the LEO orbit described in the text

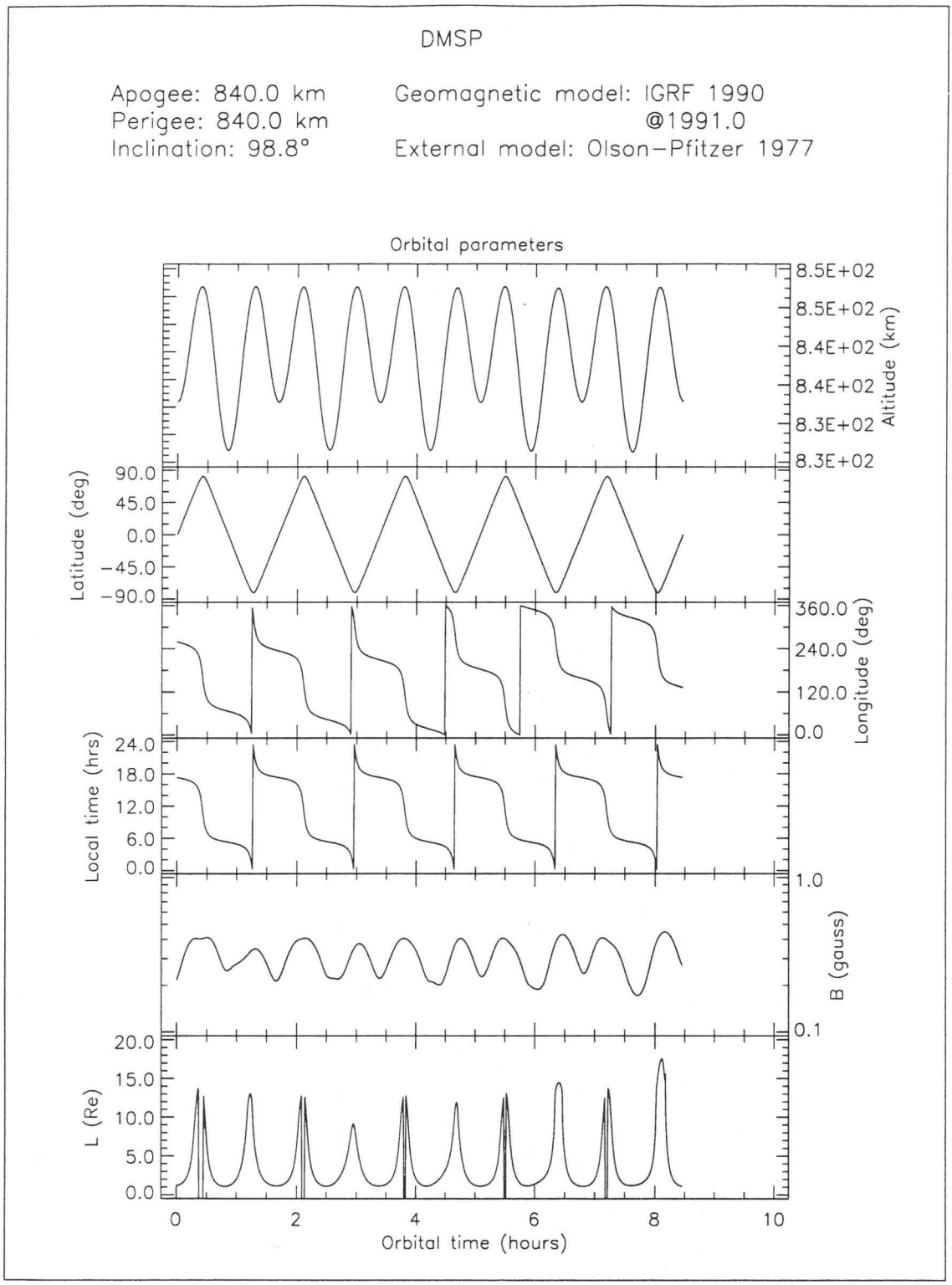

Figure 23. Geographic and magnetic coordinates for the polar orbit described in the text

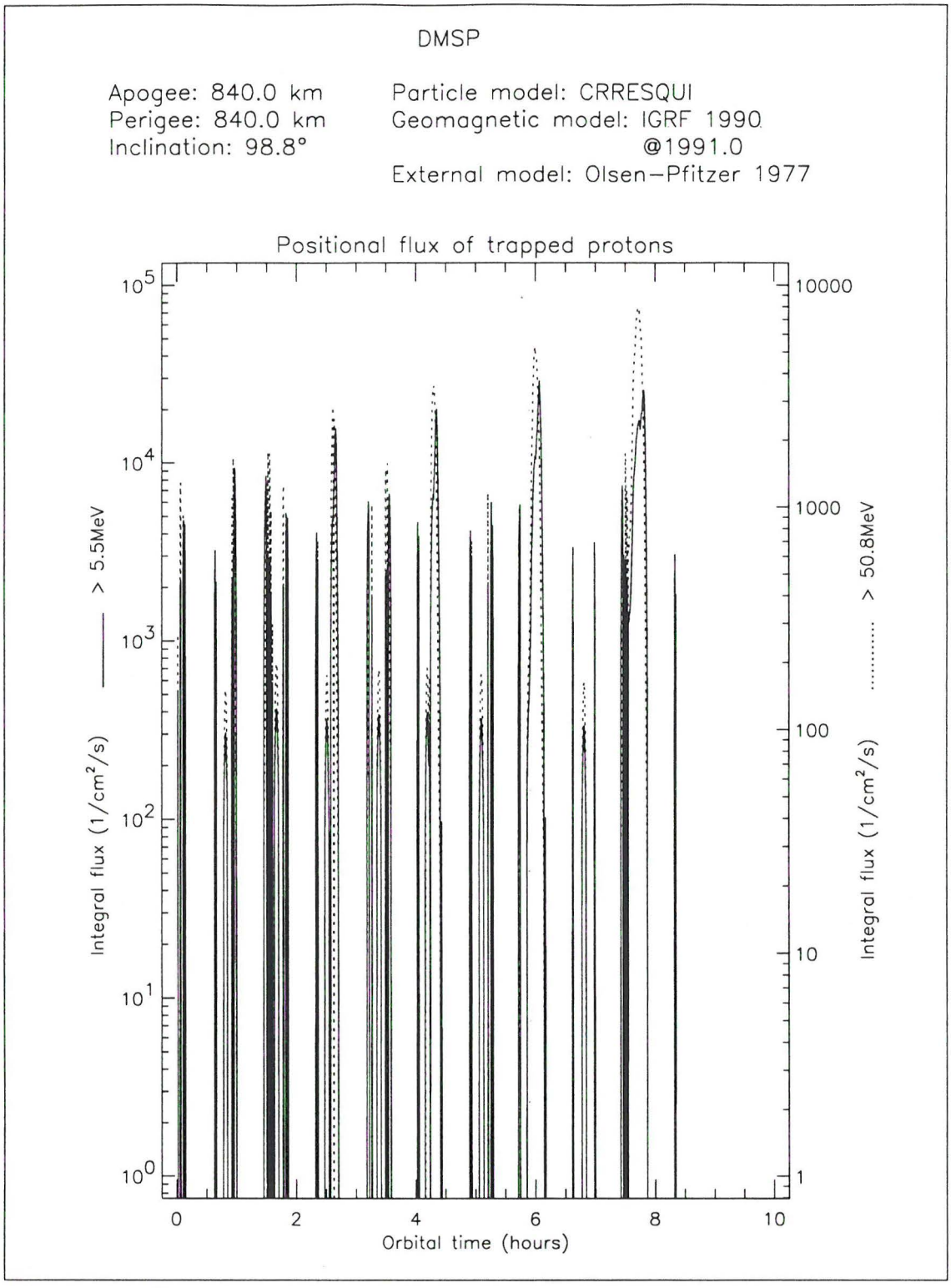

Figure 24. Differential CRRESPRO/QUIET proton flux along the polar orbit described in the text

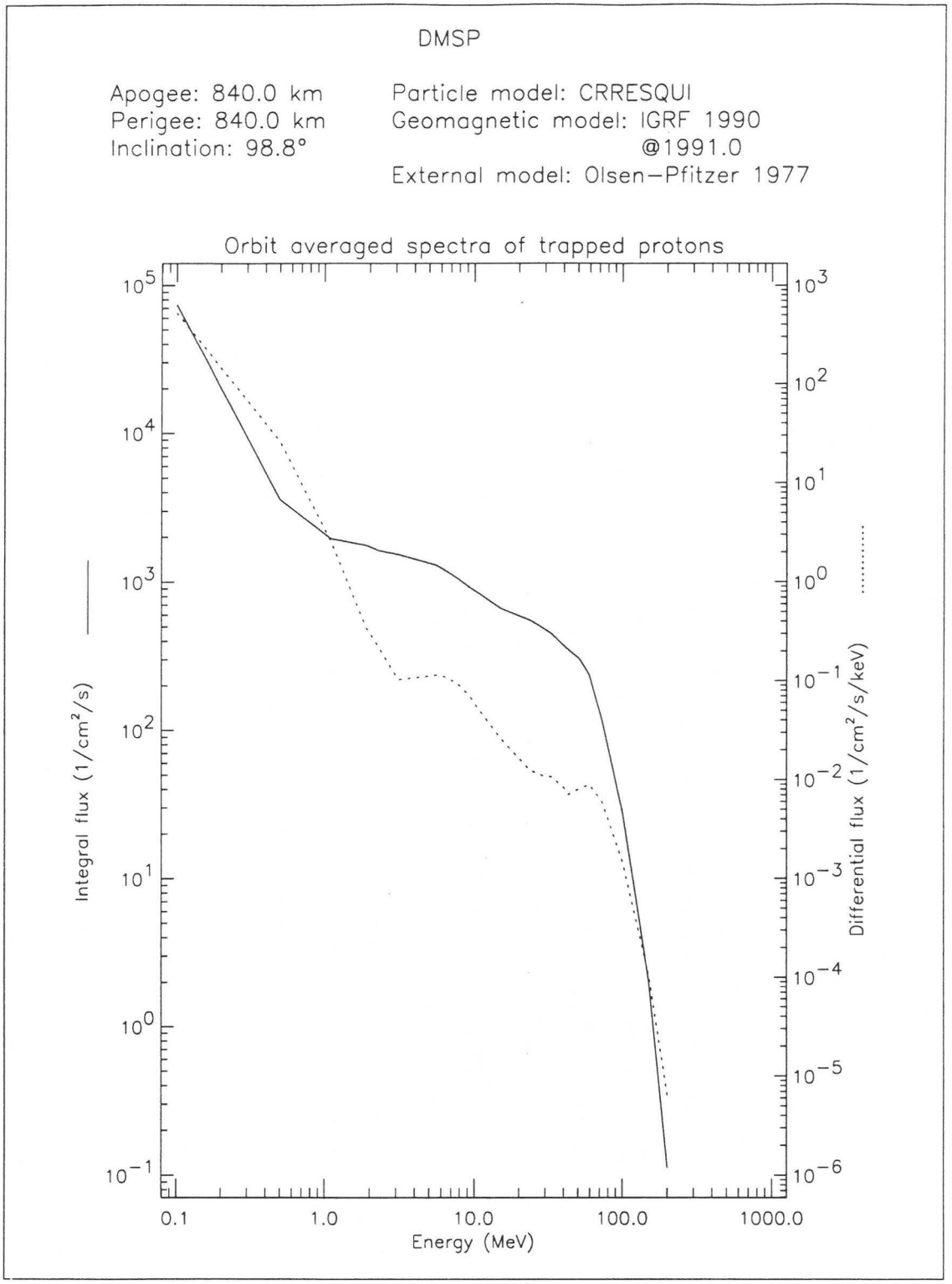

Figure 25. Integral and differential CRRESPRO/QUIET proton spectrum along the polar orbit described in the text

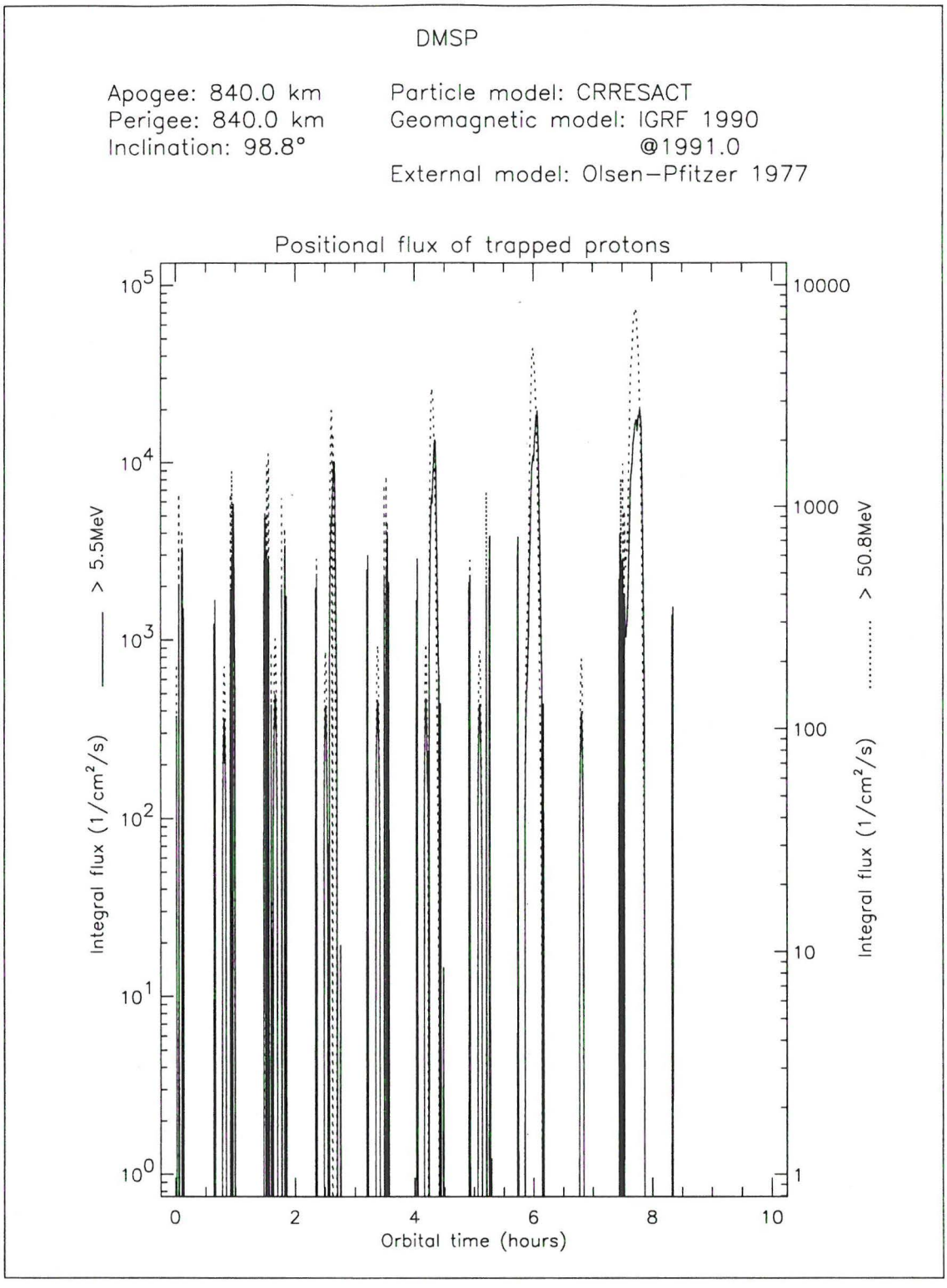

Figure 26. Differential CRRESPRO/ACTIVE proton flux along the polar orbit described in the text

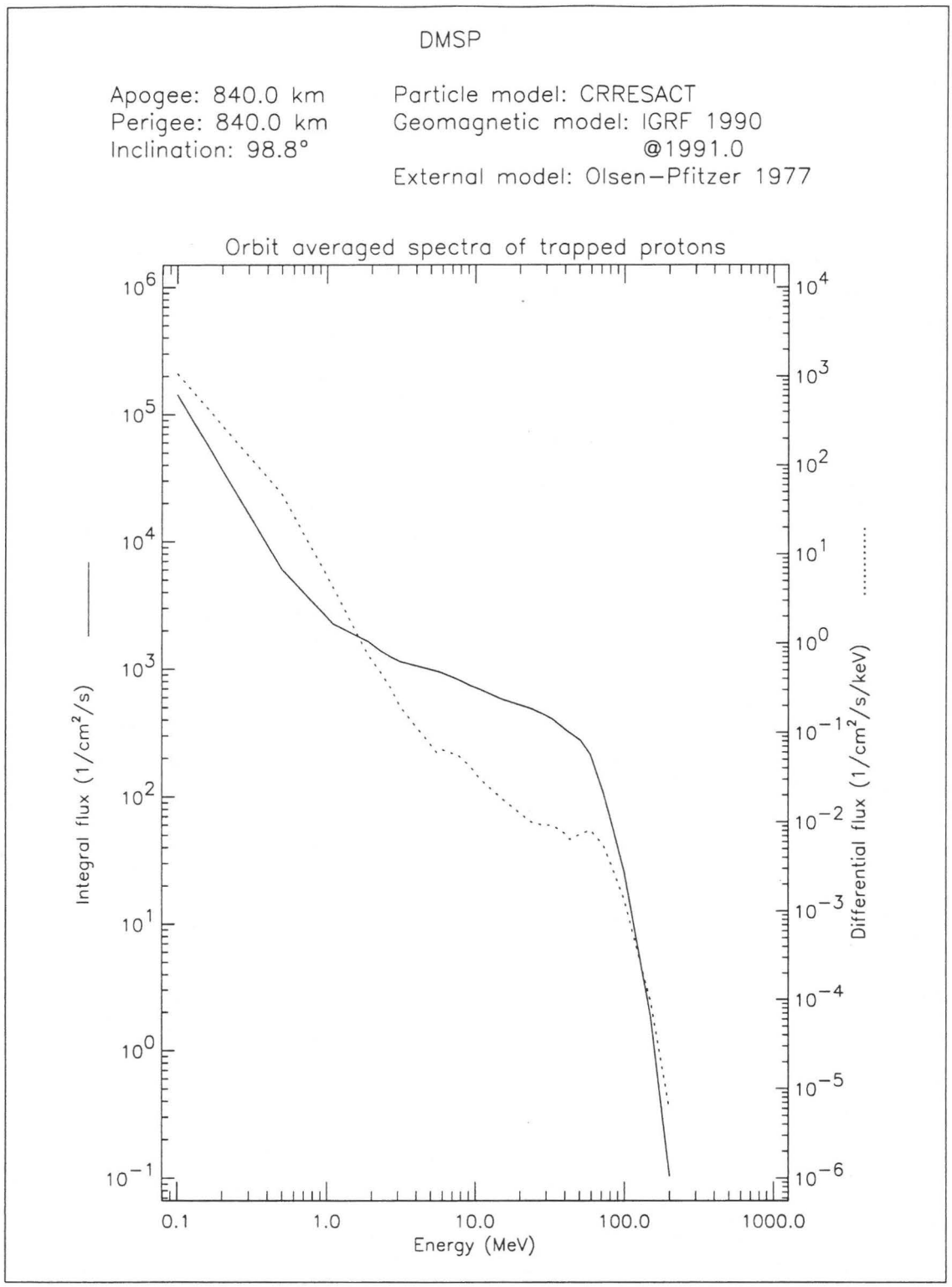

Figure 27. Integral and differential CRRESPRO/ACTIVE proton spectrum along the polar orbit described in the text

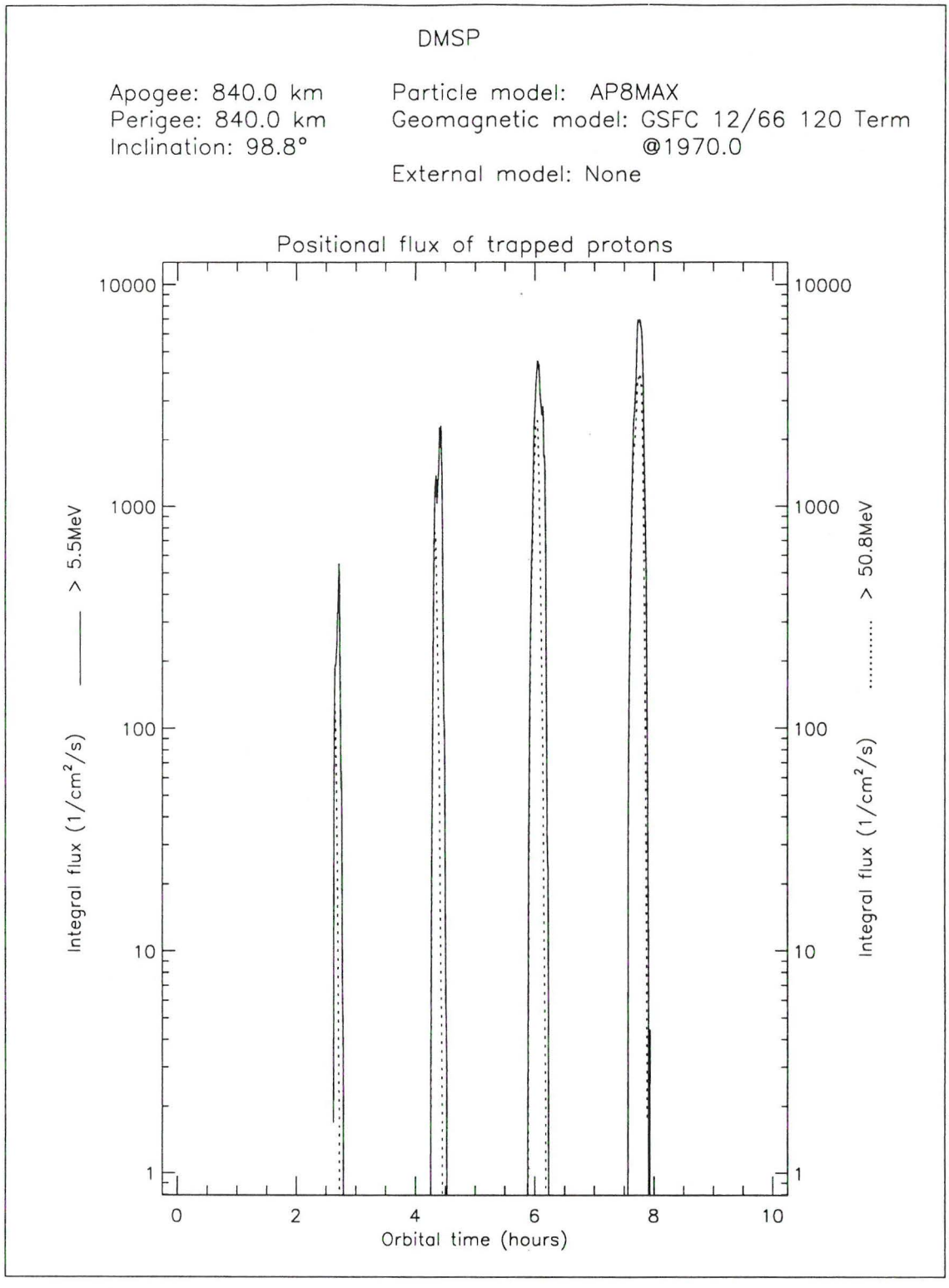

Figure 28. Differential AP-8 MAX proton flux along the polar orbit described in the text

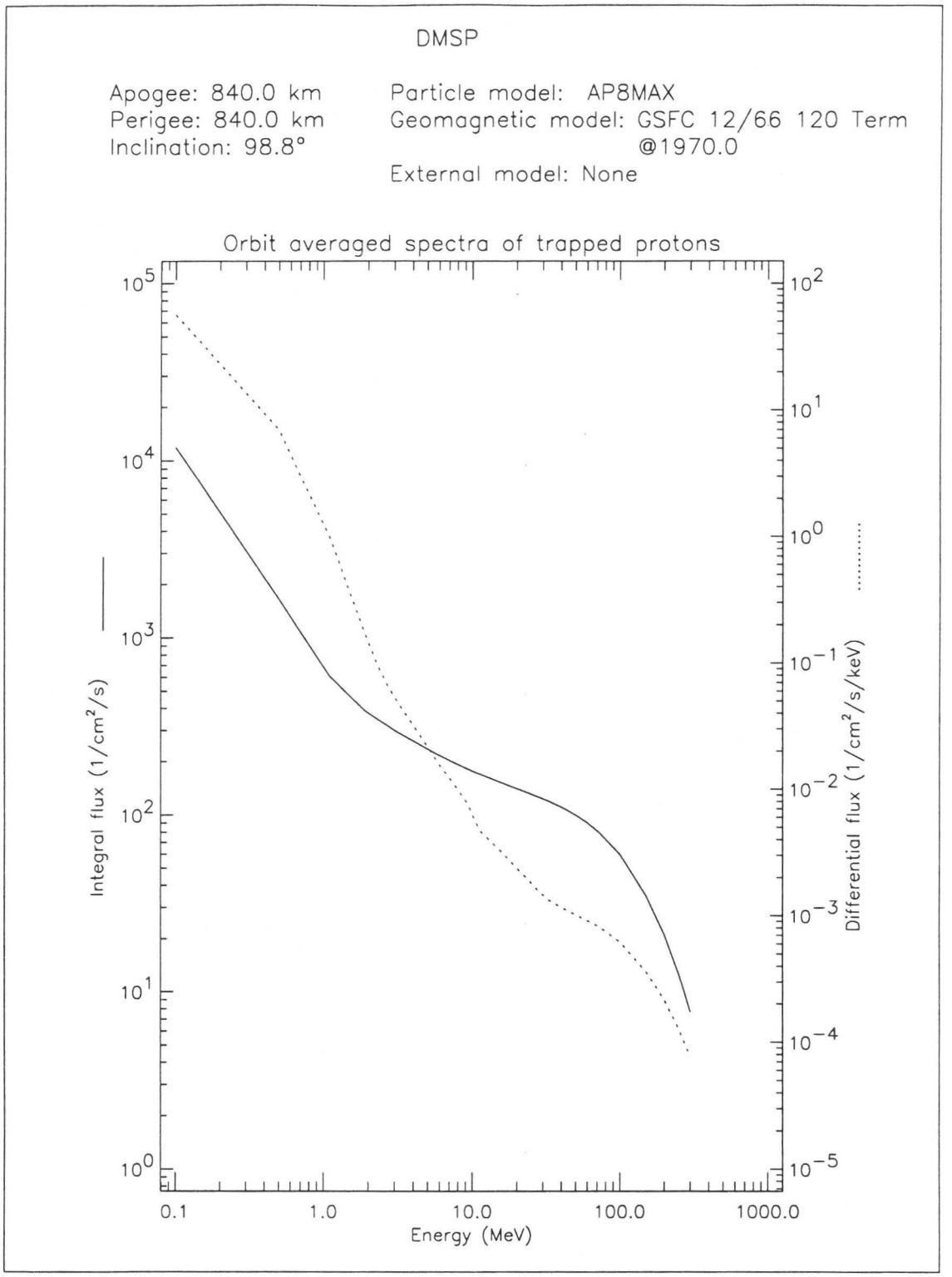

Figure 29. Integral and differential AP-8 MAX proton spectrum along the polar orbit described in the text

could be achieved in a next step provided PLGD releases the necessary software routines. In the meantime, the CRRESPRO model in TREP should not be used for low altitude analyses.

References

Badhwar, G.D., Konradi, A.: 1990, *Conversion of Omnidirectional Proton Fluxes into a Pitch Angle Distribution*, J. Spacecraft and Rockets **27**, 350–352

Cain, J.C., Hendricks, S.J., Langel, R.A., Hudson, W.V.: 1967, *A Proposed Model for the International Geomagnetic Reference Field-1965*, J. Geomag. Geoelectr. **19**, 335–355

Gussenhoven, M.S., Mullen E.G., Violet, M.D., Hein, C., Bass, J., Madden, D.: 1993, *CRRES High Energy Proton Flux Maps*, IEEE Trans. Nucl. Sci. **40**, 1450

Heynderickx, D., Lemaire, J.: 1992, *Description of the Combined Release and Radiation Effects Satellite Experiments and Data Sets*, Technical Note 4 of the TREND-2 Study, ESTEC Contract No. 9828/92/NL/FM

Heynderickx, D., Lemaire, J.: 1993, *Improvements to Trapped Radiation Software*, Technical Note 1 of the TREND-2 Study, ESTEC Contract No. 9828/92/NL/FM

McIlwain, C.E.: 1961, *Coordinates for Mapping the Distribution of Magnetically Trapped Particles*, J. Geophys. Res. **66**, 3681–3691

Meffert, J.D., Gussenhoven, M.S.: 1994, *CRRESPRO Documentation*, PL-TR-94-2218, Environmental Research Papers, No. 1158, Phillips Laboratory

Olson, W.P., Pfitzer, K.A.: 1977, *Magnetospheric Magnetic Field Modeling*, Annual Scientific Report, AFOSR Contract No. F44620-75-C-0033, McDonnell Douglas Astronautics Company, Huntington Beach, CA

Rodgers, D.J.: 1994, *Outer Radiation Belt Model Development*, Technical Note 10 of the TREND-2 Study, ESTEC Contract No. 9828/92/NL/FM

Vette, J.I.: 1991a, *The AE-8 Trapped Electron Model Environment*, NSSDC/WDC-A-R&S 91-24

Vette, J.I.: 1991b, *The NASA/National Space Science Data Center Trapped Radiation Environment Model Program (1964–1991)*, NSSDC/WDC-A-R&S 91-29

Violet, M.D., Lynch, K., Redus, R., Riehl, K., Boughan, E., Hein, C.: 1993, *Proton Telescope (PROTEL) on the CRRES Spacecraft*, IEEE Trans. Nucl. Sci. **40**, 242